Since January 2020 Elsevier has created a COVID-19 resource centre with free information in English and Mandarin on the novel coronavirus COVID-19. The COVID-19 resource centre is hosted on Elsevier Connect, the company's public news and information website.

Journal of Molecular Structure 1253 (2022) 132301

Contents lists available at ScienceDirect

Journal of Molecular Structure

journal homepage: www.elsevier.com/locate/molstr

Investigation of Cu metal nanoparticles with different morphologies to inhibit SARS-CoV-2 main protease and spike glycoprotein using Molecular Docking and Dynamics Simulation

Mohammadreza Aallaei[a], Elaheh Molaakbari[b,*], Paridokht Mostafavi[c], Navvabeh Salarizadeh[d], Rahime Eshaghi Maleksah[e], Dariush Afzali[c]

[a] Department of Chemistry, Faculty of Science, Imam Hossein University, Tehran, Iran
[b] Department of Chemistry, Shahid Bahonar University of Kerman, Kerman, Iran
[c] Department of Environment, Graduate University of Advanced Technology, Kerman, Iran
[d] Department of Cell & Molecular Biology, School of Biology, College of Science, University of Tehran, Tehran, Iran
[e] Medical Biomaterial Research Centre (MBRC), Tehran University of Medical Sciences, Tehran, Iran

ARTICLE INFO

Article history:
Received 28 August 2021
Revised 25 December 2021
Accepted 28 December 2021
Available online 31 December 2021

Keywords:
Molecular Docking
COVID-19
Molecular Dynamics Simulation
Copper NPs
Protease and Spike Glycoprotein Inhibitor

ABSTRACT

Nowadays, considering the spread of the coronavirus as a global threat, scientific research on this virus through simulation has been increasing. In this study, effect of Cu nanocluster on prevention and control of disease transmission was examined using molecular docking and molecular dynamics simulation studies on the SARS-CoV-2 main protease and spike glycoprotein. The cytotoxicity of different shapes of copper NPs and resonance changes of their surface plasmons on inactivation of the coronavirus was examined in order to control replication of coronavirus through copper NPs, active site of protease and spike glycoprotein. The simulations results showed that interactions of SARS-CoV-2 main protease and spike glycoprotein target and cylindrical and conical copper NPs ligands were more efficient than spherical copper NPs.

1. Introduction

Coronaviruses are viral pathogens with single-stranded RNA that cause significant mortality and morbidity. Information and data from different medical centers suggest that coronavirus is transmitted from person to person quickly through virus droplets or through direct /indirect contact with respiratory secretions. The prevalence of the new coronavirus revealed a new threat to human health [1-3]. Therefore, it is necessary to identify and design coronavirus inhibitors which can be available during the next epidemic [1].

The vital role of the spike protein (S protein) of coronaviruses makes this glycoprotein an important therapeutic target, because it contributes to coronavirus entry into host cells, by providing the binding and the fusion of virus into the host cell membrane. S protein is composed of two subunits, S1 which identifies and binds to the host receptors, and S2 which facilitates fusion between the viral envelope and the host cell membrane [4]. Numerous studies have explored how to target this first stage of the virus lifecycle. These methods mainly involve peptidic fusion inhibitors, anti-CoV neutralizing monoclonal antibodies, and entry receptor antagonists. However, none of these curative agents is approved for commercial use in humans [5]. Regarding the SARS-CoV-2 infection, in the absence of a clinically proved effective antiviral therapy against this disease, a combination of different drugs has been often supplemented [6–10].

Many of the approaches have used chemical and natural inhibitors, substrate mimetics and NPs that bind irreversibly to the active site of enzyme. These studies analyze inhibitory effect on enzymes, inhibition of viral replication, and structural/computational studies of inhibitors bound to enzymes [11–15]. One of the applications of nanobiotechnology is the use of nanostructures for new solutions to surface sterilization and treatment of microbial infections [16]. Antimicrobial activities of many NPs against gram-positive and gram-negative bacteria such as gold, silver and copper have been reported in previous studies. The process of adhesion and electrostatic interaction to the bacteria cell wall leads to disruption of the bacterial membrane integrity and ultimately leads to the death of microorganisms [14–16]. Copper NPs have several advantages, including availability, cost-effectiveness and easy production compared to other nanoparticles [16]. Also, copper is one of essential trace elements for hu-

* Corresponding author: Dr. Elaheh Molaakbari
E-mail address: e.molaakbari@gmail.com (E. Molaakbari).

https://doi.org/10.1016/j.molstruc.2021.132301
0022-2860/

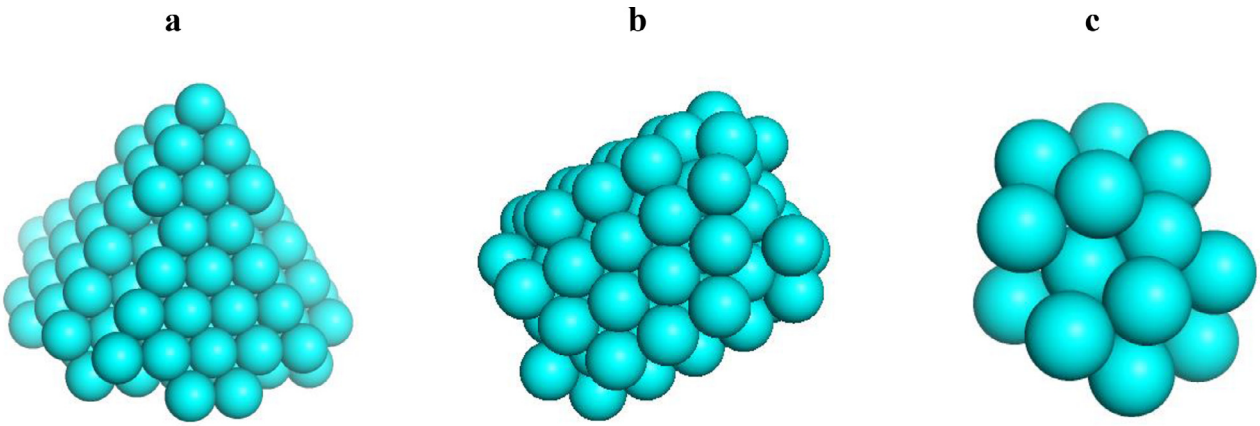

Figure 1. a) Cone b) Cylindrical c) Spherical copper NPs molecular structure as Ball and Bond type in position drawn by MVD 6.0.

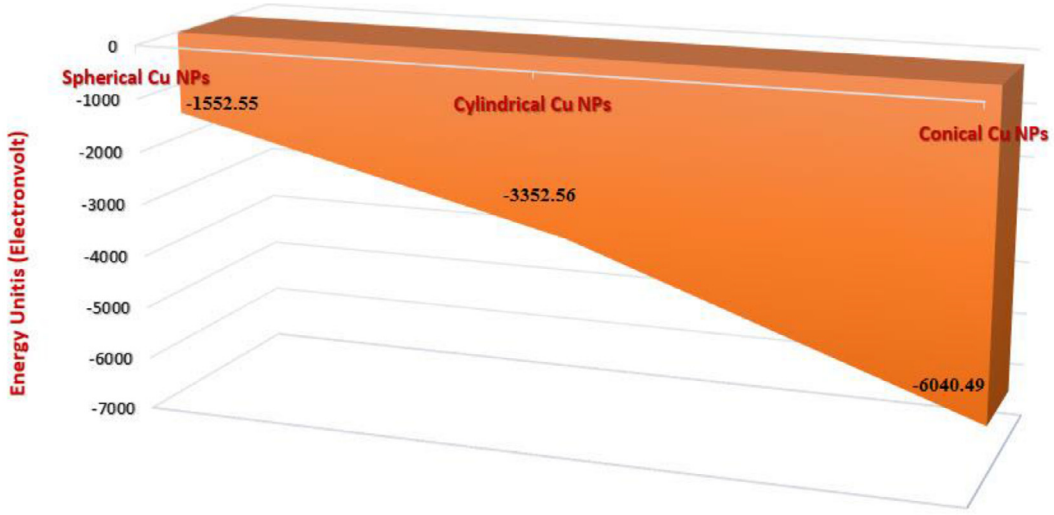

Figure 2. The energy units of spherical Cu NPs, cylindrical Cu NPs and conical Cu NPs.

mans. Cu^{2+} has the potential of neutralizing infectious viruses, on enveloped single/double-stranded DNA and RNA viruses such as bronchitis virus, poliovirus, human immunodeficiency virus type 1 [17]. The antimicrobial activity of nanoparticles varies according to their size and morphology. In this research, the impact of various forms of copper including spherical, conical and cylindrical shapes on inactivation of viral main protease was investigated through computational simulations. These nanoparticles interact electrostatically with viral protease with negative net charge due to the positive copper metal. This interaction may be inactivated virus inhibition of a major enzymes of virus.

2. Method computational

2.1. Ligand preparation

The unit cells of copper NPs were made according to the library of Materials Studio 2017 software [18] and molecular mechanics optimizations such as, MM+ force field with Hyperchem software was applied to optimize the molecular structure (to reach its real and natural state) and then, saved in Mol2 format which can be used for molecular docking. MD simulations was carried out under NVT conditions (constant particle number, constant volume, and constant temperature) with the Berendsen thermostat constant was used for fixing the temperature of the system at 298 K and NPT conditions (constant particle number, constant temperature, and constant pressure) with the Parrinello–Rahman pressure coupling method was applied to fix the pressure at 1 bar with a gap time of 1 fs to achieve a stable state. Afterwards, the simulation was performed in the time of 10 ns and ensemble atomic simulation on different shapes of copper NPs. Figures 1a-c and 2 show structures and total energies of the different shapes of copper NPs ligands optimized using molecular dynamics.

2.2. Target/Receptor preparation

Proteins used in this study are the ones which are involved in the mechanism of action of the SARS-CoV-2 such as main protease and spike glycoprotein. In this section, first the structure of the target proteins (6M03 and 6ZGG) was downloaded in PDB format from the RCSB protein data bank (https://www.rcsb.org/). Figures 3a and b show the molecular structure of the targets. In order to prepare suitable situation for molecular docking, additional structures in the PDB file were removed in the downloaded file using Discovery Studio software, however, for more accurate molecular docking, water molecules and cofactors were not omitted in the docked PDB file so that the conditions are close to their normal state.

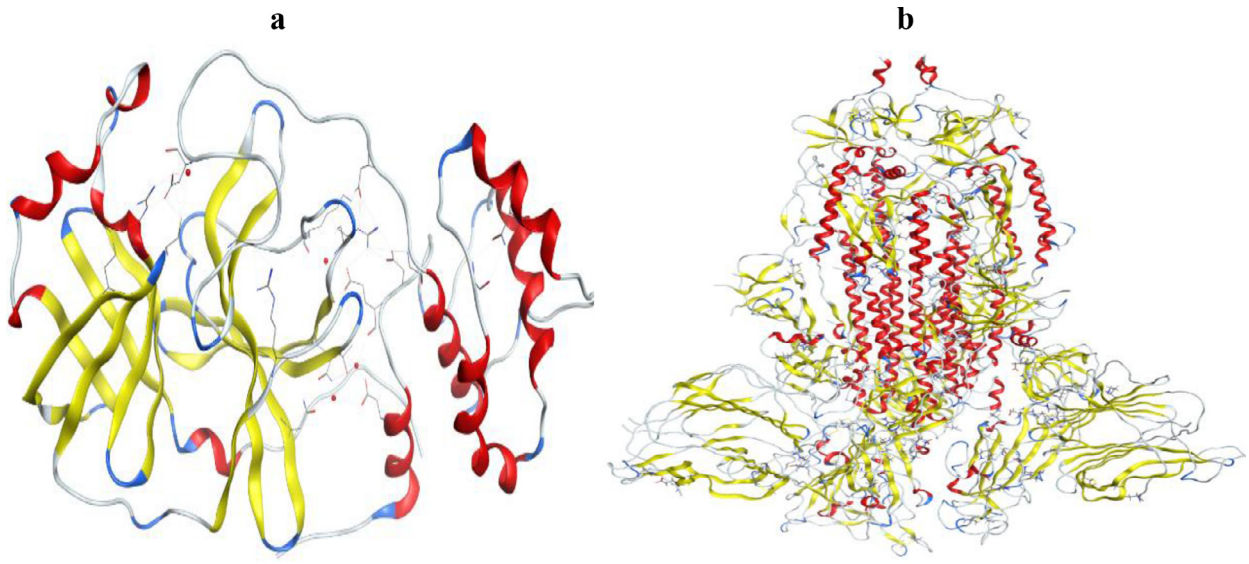

Figure 3. The α helices and β strands of a) 6M03 protein (3D) b) 6ZGG protein (3D) are represented as coils (red) and arrows (blue) respectively.) with the selected crystal structure drawn by MOE 2011.

2.3. Molegro Virtual Docker 6.0 (MVD)

Structures of the protein and the compounds were prepared using the module of "preparation molecule for docking". Applying "Detect cavities" module, appropriate locations on receptor to interact with the compounds were determined. Grid resolution of 0.30Å, maximum iteration of 1500 and maximum population size of 50 were set as docking parameters. The internal ES (Internal electrostatic Interaction), sp^2-sp^2 torsions and the internal H-bond interactions were set to evaluate the binding affinity and interactions of the compounds with the M^{pro}. Simplex evolution was set to maximum steps of 300 with neighborhood distance factor of 1. Ten sets of docking were run followed by post dock energy minimization applying the Nelder-Mead Simplex Minimization. The final outcomes were analyzed using Molegro Molecular Viewer 7.0 and the best interacting compound was selected from each dataset. The accuracy of AUTODOCK VINA software was nearly 78% higher than AUTODOCK4.2 and also the accuracy drawn by MVD 6.0 software was close to 87% compared to other docking software [19–21]. Figures 4a and b show the cavities of the targets (6M03 and 6ZGG) that interact with the ligand and dock there, respectively.

2.4. Molecular Operating Environment 2011 (MOE)

Receptor and ligands were prepared with the default 3D protonation procedure in MOE, version 2011 (Chemical Computing Group Inc; Montreal, QC, Canada: 2011. And Vilar, Cozza & Moro, 2008). Docking was performed applying all default parameters with Triangle Matcher, retaining 5 poses and GBVI/WSA rescoring. Figures 5a and b show the active sites of the targets (6M03 and 6ZGG) that interact with the ligand and dock there, respectively. After run, the best poses related to ligands and targets were displayed. Among the poses with level of energy, the best pose with the least amount of energy was selected to be used to obtain Pharmacophore topics.

2.5. Autodock Vina

Receptor structures were downloaded from PDB. Water molecules, heteroatoms and ligands were removed in Discovery Studio Software and converted to PDB format. The ligand files were also saved in PDB format, and then the receptor structures were placed as input in AutoDock Tools software, where hydrogen added to the protein structures. In the next step, the load calculations were performed automatically, after which the ligand was formatted. The PDB is called and ready for docking. The settings related to the Grid box in size X = 126, Y = 126, Z = 126 and Cut-off = 1 A° were selected and stored and molecular docking was performed.

2.6. Molecular dynamics (MD) simulation

Molecular dynamic (MD) simulation was performed to further analysis of the best docking modes according to the receptor-ligand interactions. MD simulation was performed using GROMACS program version 2019.1 and the GROMOS 54A7 force field was applied for all simulations. The system was stabilized by adding water and Na^+/Cl^+ ions. Energy minimization was performed for 50000 steps with the GROMOS 54A7 force field. The system was equilibrated in the canonical (NVT) ensemble for 1 ns and in the isothermal–isobaric (NPT) ensemble equal to 1 bar. The Berendsen thermostat constant was used for fixing the temperature of the system at 300 K. The Parrinello–Rahman pressure coupling method was applied to keep the pressure of the system at fixed 1 bar with a gap time of 2 fs to achieve a stable state.

In order to inspect investigated ligands and achieve higher efficiency, molecular dynamics of considered targets 6M03 and Chain A (6ZGG) was performed for 100 to 110 nano seconds using Gromacs software and redocking was performed in the active site where had been docked before since molecular docking for protein code spike glycoprotein SARS-COV-2 (6ZGG) had been in active and binding site of chain A before molecular dynamic and for accelerating molecular dynamic analysis Chain A protein code spike glycoprotein SARS-COV-2 (6ZGG) was used. Furthermore, a time of 110 nanoseconds was considered to equilibrate of the system.

The LINCS algorithm was applied to calculate the long-range electrostatic interactions using the Particle-Mesh-Ewald (PME) method.

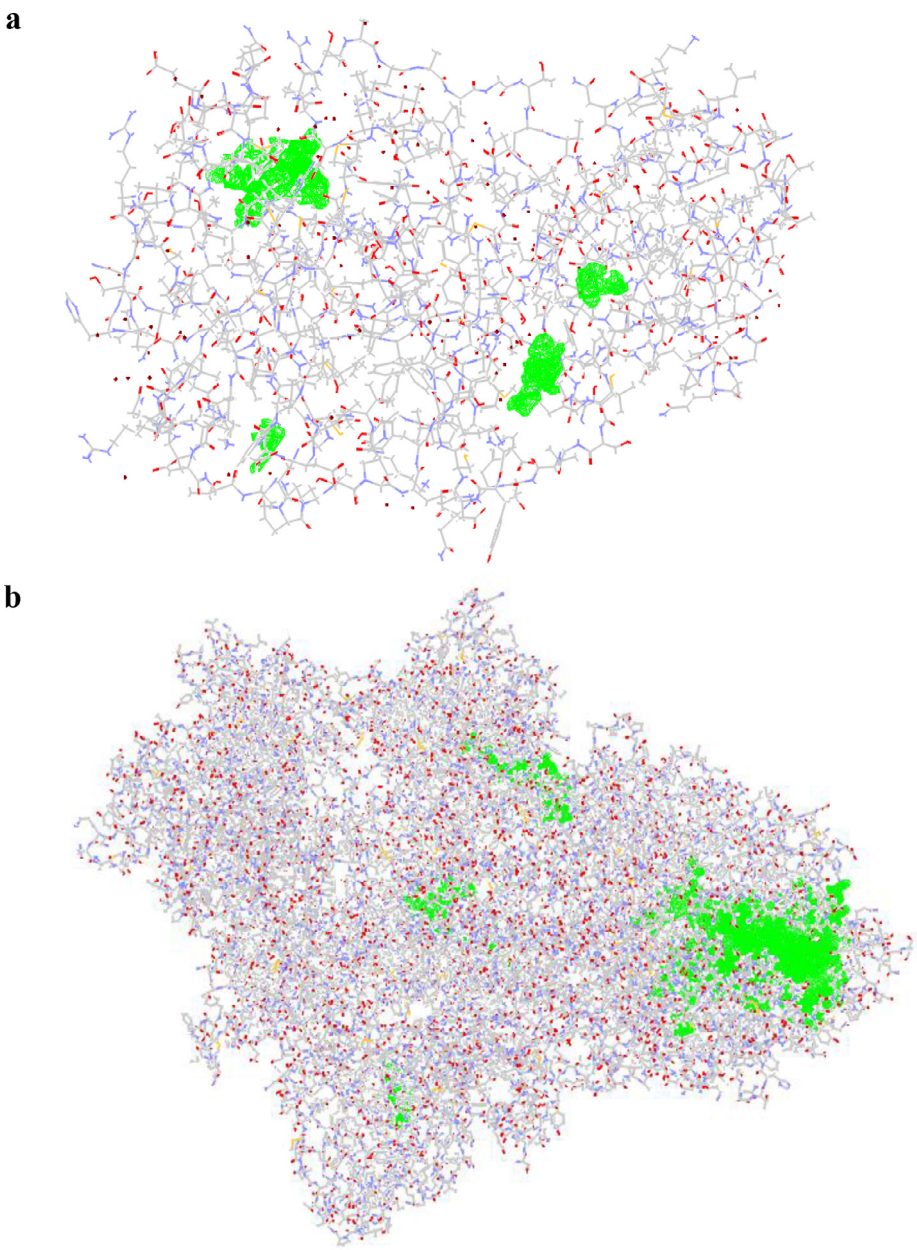

Figure 4. Area of molecular structure of a) 6M03 protein b) 6ZGG protein. The cavities of the targets that interact with the ligand and dock there green color drawn by MVD 6.0

3. Results and Discussion

3.1. MVD Molecular docking studies related to main protease (M^{pro}) and spike glycoprotein

In order to understand the interactions of our desired 3 compounds with main protease and spike glycoprotein active sites better, the docking modelling studies were carried out by MVD and the docking results are listed in Tables 1 and 2. Conformation of docked Copper NPs ligand with main protease and spike glycoprotein were analyzed in terms of Total Energy or MolDock Score values that were dominated by the negative energy values, implying that the binding effects of the compounds were spontaneous. The values of Free Total Energy of MolDock Score numbers were -137. 21, -77. 739 and -48. 239 for conical, cylindrical and Spherical Copper NPs docked to main protease respectively. The data in Table 2 show that MolDock Score of conical, cylindrical and Spherical Copper NPs interacted with spike glycoprotein was -148. 09, -114. 044 and -83. 751 respectively. The calculated minimum relative Free Total Energy values score suggest that they are reasonably interacted to macromolecules. Comparing the Free Total Energy or MolDock Score of compounds with main protease and spike glycoprotein that conical Copper NPs was more effective compared with other compounds.

Table 1
Resulted parameters from involvement between copper NPs ligands and SARS-COV-2 main protease of MVD.

Compound	Mol dock Score	ET
cone copper NPs	-137.212	-87.284
cylindrical copper NPs	-77.739	52.995
spherical copper NPs	-48.239	116.664

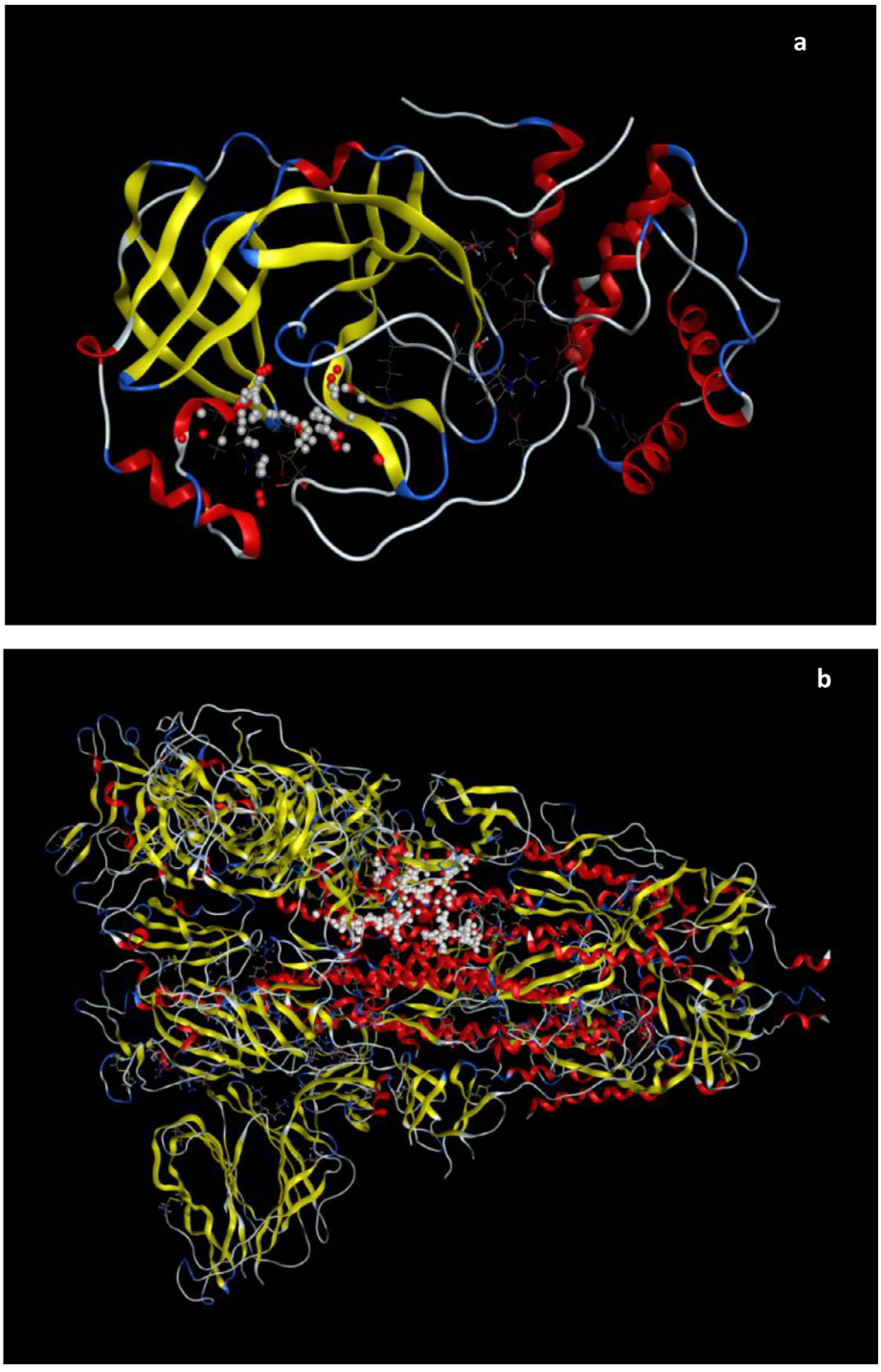

Figure 5. The active sites molecular structures of a) 6M03 protein b) 6ZGG proteins. The docking areas are shown as white and red ball drawn by MOE 2011.

Table 2
Resulted parameters from involvement between copper NPs ligands and SARS-COV-2 spike glycoprotein of MVD.

Compound	Mol dock Score	ET
cone copper NPs	-148.09	-148.09
cylindrical copper NPs	-114.044	-114.043
spherical copper NPs	-83.751	-83.751

Furthermore, Figures 6a-f show the most interacted shape of copper NPs ligand in the active site of main protease. The obtained data from docking analysis showed that conical Copper NPs were interacted with amino acids of the main protease (PDB ID, 6M03) using Val A104, Arg A105, Ile A106, Gln A107, Gln A110, Asp A248, Ile A249, Phe A294, Pro A252 (Figures 6a and d). cylindrical Copper NPs were interacted with amino acid residues include Ile A249, Pro A252, Pro A293, Phe A294, and Val A294 in active site of main protease (Figures 6b and e). Meanwhile, amino acids of main protease such as Gln A110, Ile A249, Thr A292, Pro A293, Phe A294 were

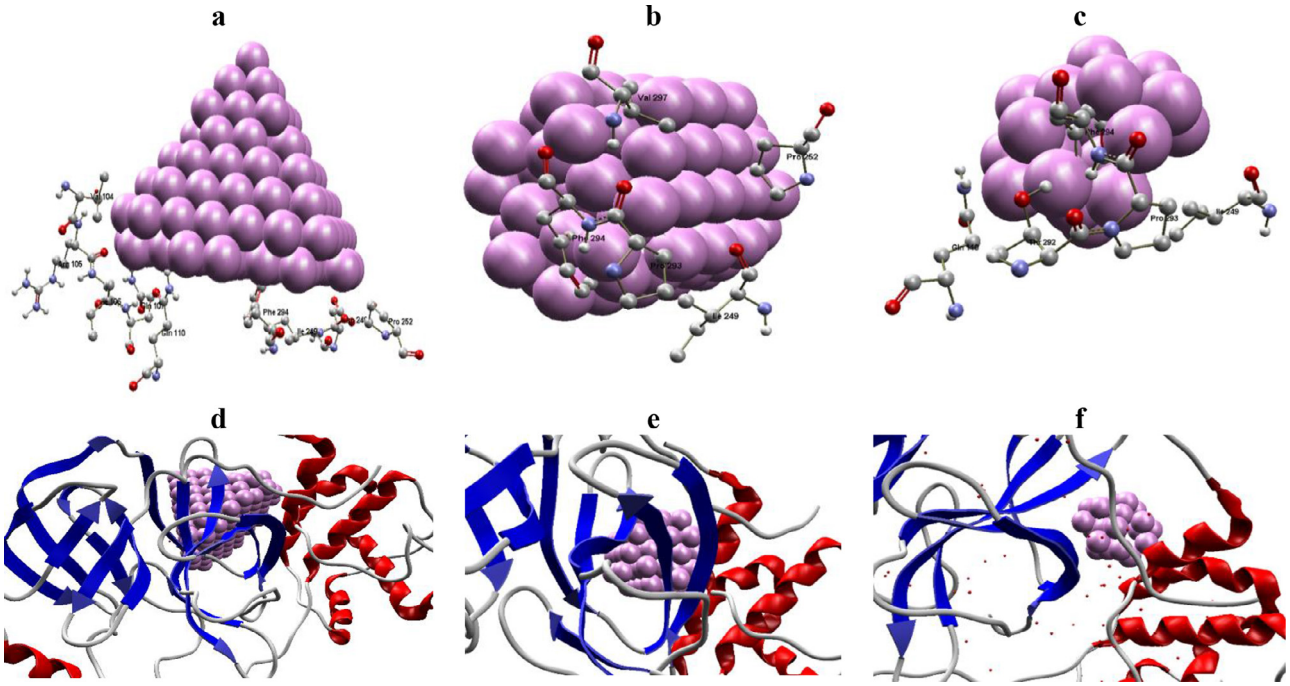

Figure 6. Schematic of the molecular docking between the Copper NPs ligands and the 6M03 receptor along with the pharmacophore and ligand map drawn by MMV 7.0.

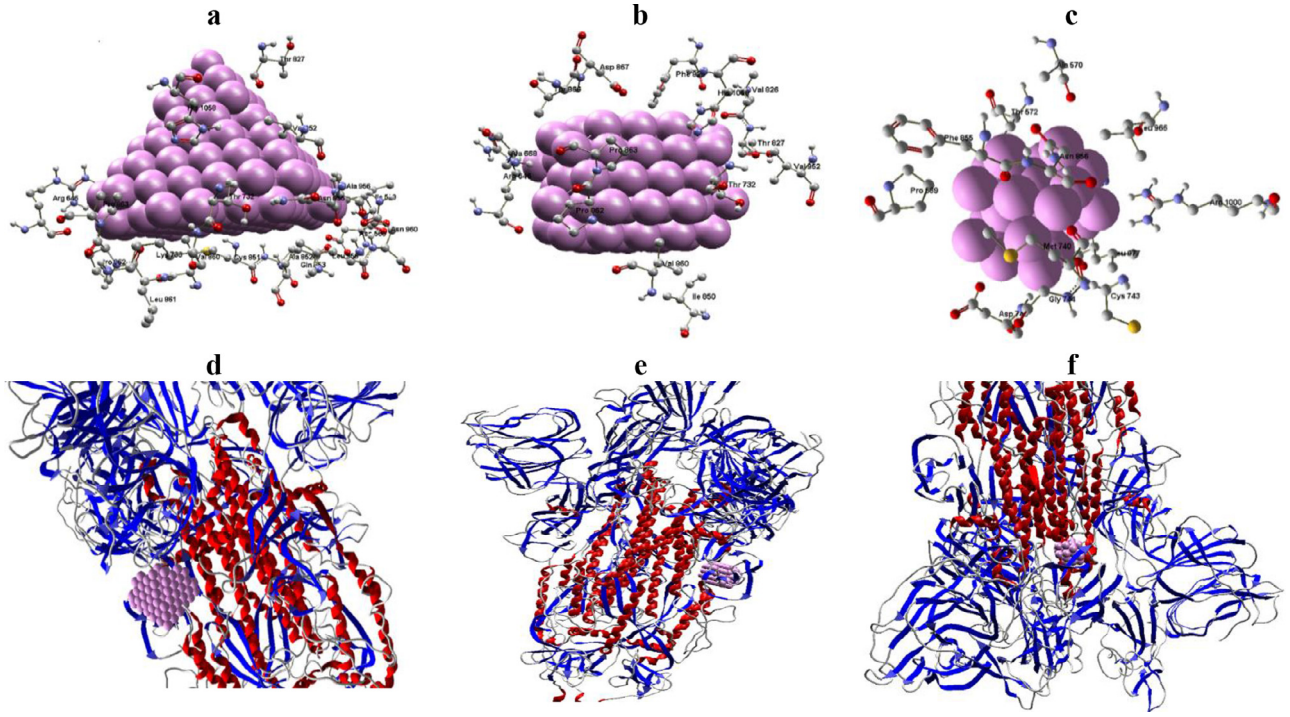

Figure 7. Schematic of the molecular docking between the Copper NPs ligands and the 6ZGG receptor along with the pharmacophore and ligand map drawn by MMV 7.0.

interacted with the spherical copper NPs (Figure 6c and Figure 6f). Interactions of copper NPs with residues of spike glycoprotein were shown in Figure 7a-c. Figure 7d-f indicates copper NPs embedded in the active site of spike glycoprotein (PDB ID, 6ZGG). Furthermore, conical copper NPs interacted with Thr A827, Val A952, His A1058, Thr A732, Ala A956, Asn A955, Lys A733, Pro A862, Val A860, Leu A861, Pro A863, Pro A862, Arg A646, Val A860, Leu A959, Asn A960, Cys A851, Gln A853 Ala A852, Asp A568, Ile A569 in spike glycoprotein respectively. On the other hand, cylindrical Copper NPs was docked into Spike glycoprotein using Arg A646, Ala A668, Thr A866, Asp A867, Phe A823, His A1058, Val A826, Thr A827, Val A952, Thr A732, Ile A850, Val A860, Pro A862, Pro A863. Spherical Copper NPs/spike glycoprotein complex was interacted with Pro A589, Phe A855, Thr A572, Ala A570, Leu A966, Asn A856, Arg A1000, Leu A977, Met A740, Cys A743, Gly A744, Asp A746.

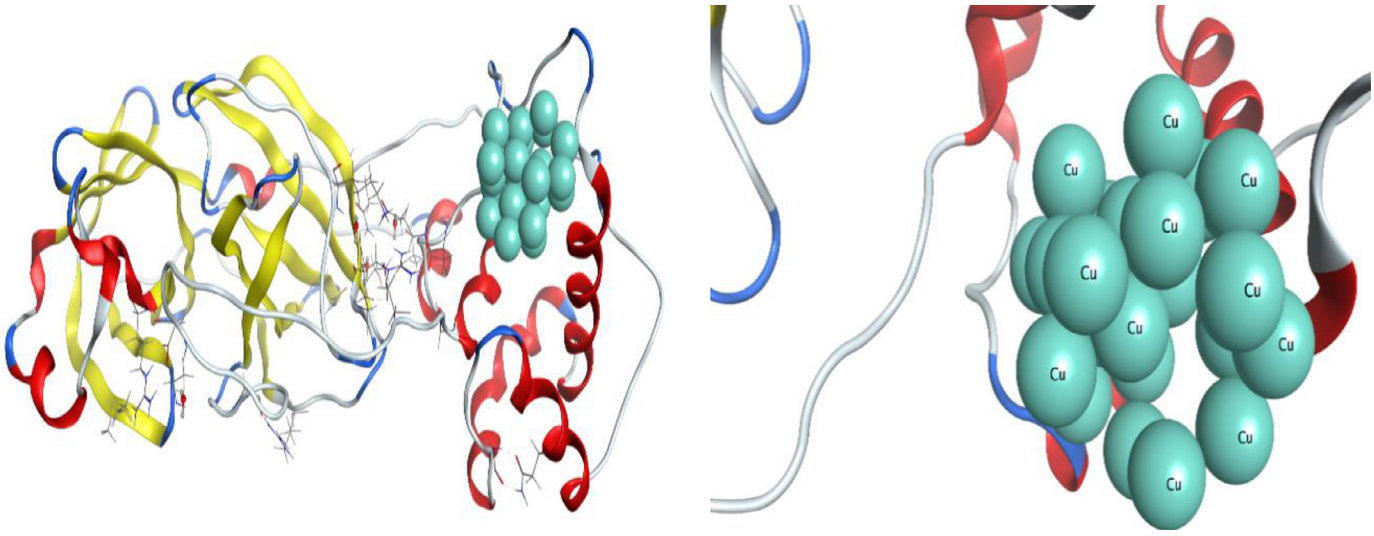

Figure 8. Schematic of the molecular docking between the Spherical copper NPs ligand and the 6M03 receptor along with the pharmacophore drawn by MOE 2011.

Table 3
The best result of the docking between copper NPs ligands and SARS-COV-2 main protease based on S, RMSD and E-refine

E-refine (Kcal/mol)	RMSD	S (Kcal/mol)	Compound
-5.83	0.36	-5.83	cone copper NPs
-10.19	0.77	-10.19	cylindrical copper NPs
-7.10	1.01	-7.10	spherical copper NPs

Table 4
The best result of the docking between NPs Copper and SARS-COV-2 spike glycoprotein based on S, RMSD and E-refine

E-refine (Kcal/mol)	RMSD	S (Kcal/mol)	Compound
-0.47	0.58	-0.47	cone copper NPs
-10.54	0.66	-10.54	cylindrical copper NPs
-9.31	0.82	-9.31	spherical copper NPs

Table 5
Resulted parameters from involvement between copper NPs ligands and SARS-COV-2 main protease of Autodock Vina.

Compound	Affinity(Kcal/mol)
cone copper NPs	-13.2
cylindrical copper NPs	-11.7
spherical copper NPs	-7.7

Table 6
Resulted parameters from involvement between copper NPs ligands and SARS-COV-2 spike glycoprotein of Autodock Vina.

Compound	Affinity(Kcal/mol)
cone copper NPs	-18.8
cylindrical copper NPs	-17.1
spherical copper NPs	-8.6

3.2. MOE Molecular docking studies related to M^{pro} and spike glycoprotein

Tables 3 and 4, show the best results of the dock between copper NPs ligands and the targets (6M03 and 6ZGG). Based on the obtained or acquired data in these tables, it can be concluded that the cylindrical and conical copper NPs ligands have the best involvement with the 6M03 and 6ZGG receptors which are in the most stable states with these receptors, however Spherical Copper NPs did not get interacted with the 6M03 and 6ZGG receptors well. This will avoid observation of the necessary stability in the system. Figures 8-13 show molecular docking between the copper NPs ligands and the 6M03 and 6ZGG targets that showed the ligand map and pharmacophore in MOE. Figure 10 is shown interactions of conical copper NPs molecules with PHE 294 amino acid residues of 6M03 receptor.

Figure 11 is shown interactions of spherical copper NPs molecules with Ser A975, Val A976 and Leu A977 amino acid residues of 6ZGG receptor. Figure 12 shows interactions of cylindrical copper NPs molecules with Pro A862 and Val A860 amino acid residues of 6ZGG receptor. It is obviously proved that cylindrical and conical copper NPs have greater effects of inactivating the virus due to their increased resonance of surface Plasmons resulting in its sharp tip. However spherical copper NPs are not as effective as conical and cylindrical forms because of less surface Plasmon resonance.

RMSD analysis between NPs Cu (spherical, cylindrical and cone) and targets (6M03 and 6ZGG) was performed, which reveals that nearly all three NPs were stable and shown RMSD calculations within the range of 0. 58-0. 82 Å of 6M03 and 0. 36-1. 01 Å of 6ZGG Figure 14a-b.

3.3. Autodock Vina Molecular docking studies related to M^{pro} and spike glycoprotein

To understand the involvement of our 3 desired compounds with main protease and spike glycoprotein active sites, the docking modelling studies were carried out with Autodock Vina .The docking results are listed in Tables 5 and 6. Conformation of docked copper NPs with main protease and spike glycoprotein were analyzed in terms of affinity values and were dominated by the negative energy values, implying that the binding effects of the compounds were spontaneous. The values Energy of affinity were -13.2, -11.7and -7.7 for conical, cylindrical and spherical copper NPs docked to main protease respectively (table 5). The data in Table 6 show that affinity of conical, cylindrical and Spherical Copper NPs interacted with spike glycoprotein were -18.8, -17.1 and -8.6 respectively. The calculated minimum relative affinity values

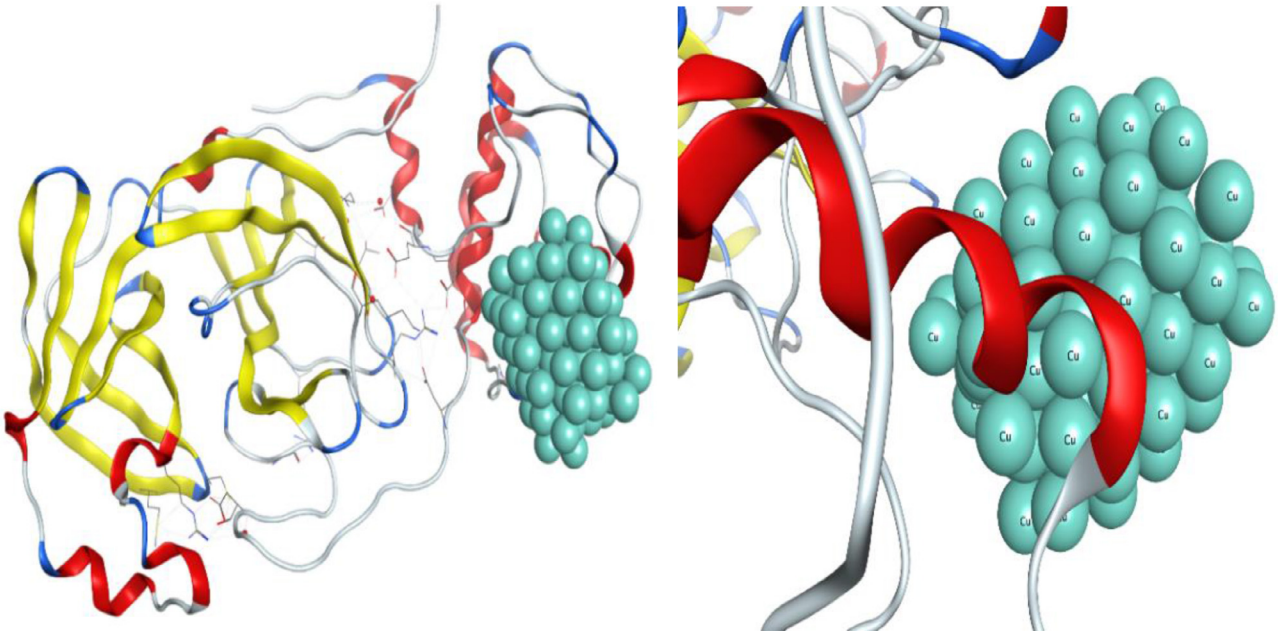

Figure 9. Schematic of the molecular docking between the Cylindrical Copper NPs ligand and the 6M03 receptor along with the pharmacophore drawn by MOE 2011.

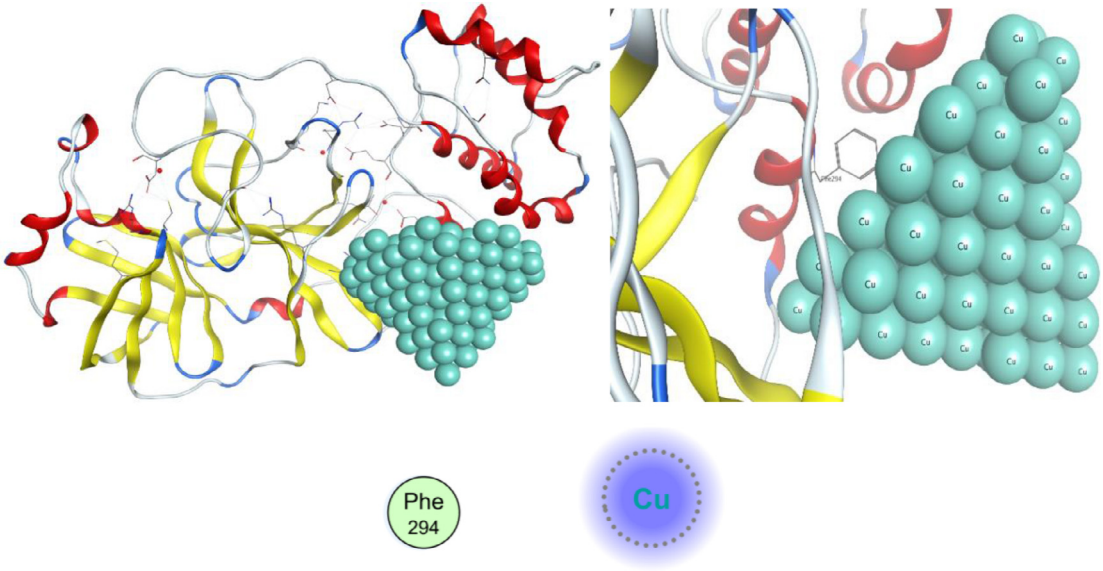

Figure 10. Schematic of the molecular docking between the Cone Copper NPs ligand and the 6M03 receptor along with the pharmacophore and ligand map drawn by MOE 2011.

score suggest that they were reasonably interacted with macromolecules. After comparing the affinity of compounds with main protease and spike glycoprotein it was concluded that conical copper NPs were more effective than other compounds to main protease and spike glycoprotein.

Figures 15a-f show the highest level of involvement of copper NPs ligand at the active site of main protease. The obtained data from docking analysis showed that conical copper NPs interacted with amino acids of the main protease (PDB ID, 6M03) using Val A125, Tyr A126, Ser A139, Gly A138, Lys A137, Gln A127, Glu A288, Lys A5, Arg A4, Ser A284 and Gly A283(Figures 16a and d). cylindrical copper NPs interacted with amino acid residues Lys A137, ArgA131, AspA197, Thr A196, Thr A198, Thr A199, Tyr A239, Asn A238, Tyr A237, Leu A286 and Leu A272 in active site of main protease (Figures 15b and e). Meanwhile, interacted between the Spherical Copper NPs and main protease were dominated by Glu A288, Asp A289, Lys A137, Thr A199, Arg A131, Leu A287, Leu A286, Tyr A239, Thr A198, Asn A238, Asp A197, Lys A137, Arg A131 in Figure 16c and f.

3.4. Study of molecular dynamics on Main Protease SARS-COV-2 (6M03) and spike glycoprotein Chain A SARS-COV-2 (6ZGG) codes

The results showed that the complexes formed between the copper nanoparticles and the studied targets are more stable in the case where molecular dynamics is performed than in the case where molecular dynamics is not performed. Also, conical copper nanoparticles are more stable than cylindrical copper nanoparticles

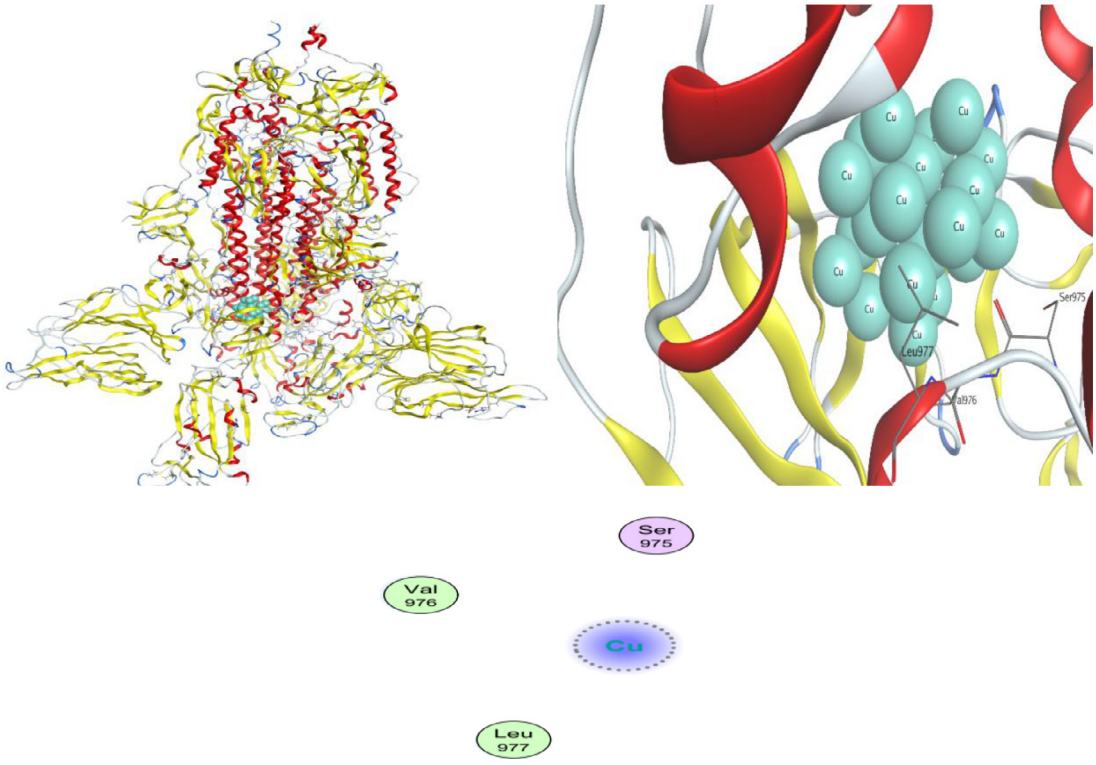

Figure 11. Schematic of the molecular docking between the Spherical Copper NPs ligand and the 6ZGG receptor along with the pharmacophore and ligand map drawn by MOE 2011.

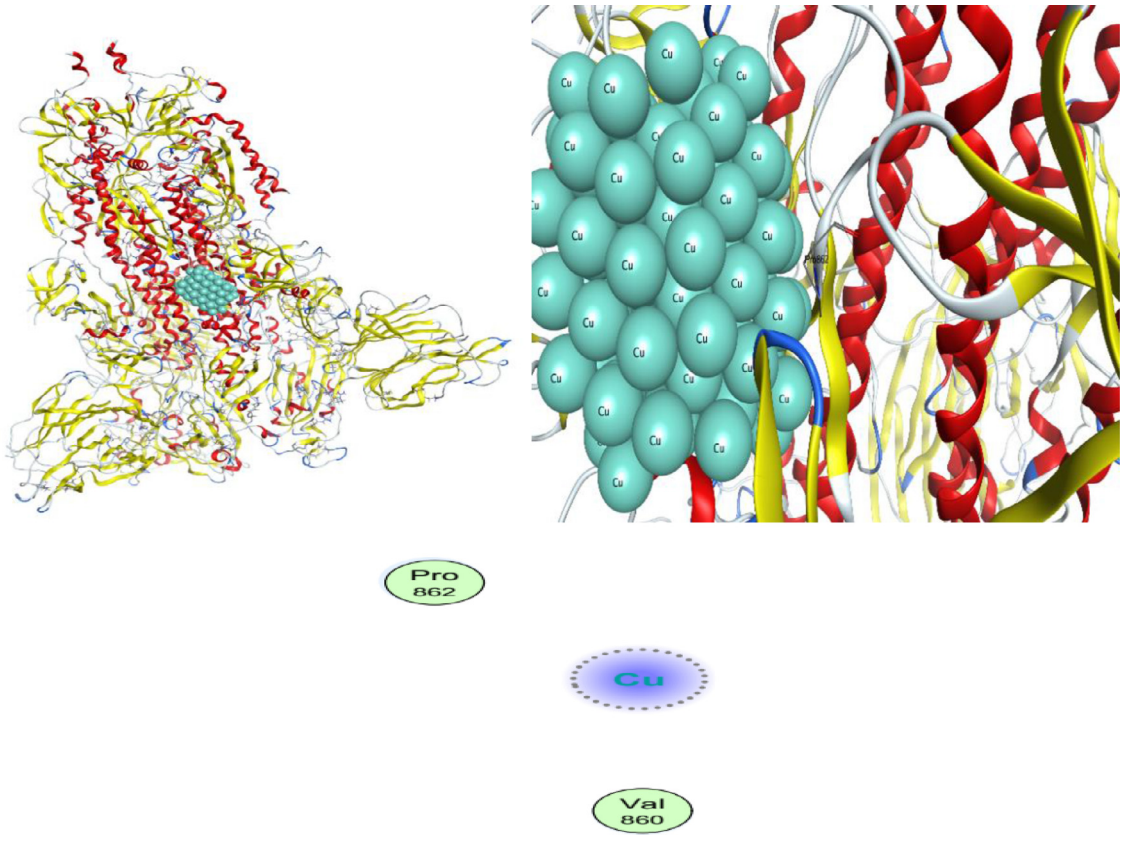

Figure 12. Schematic of the molecular docking between the Cylindrical Copper NPs ligand and the 6ZGG receptor along with the pharmacophore and ligand map drawn by MOE 2011.

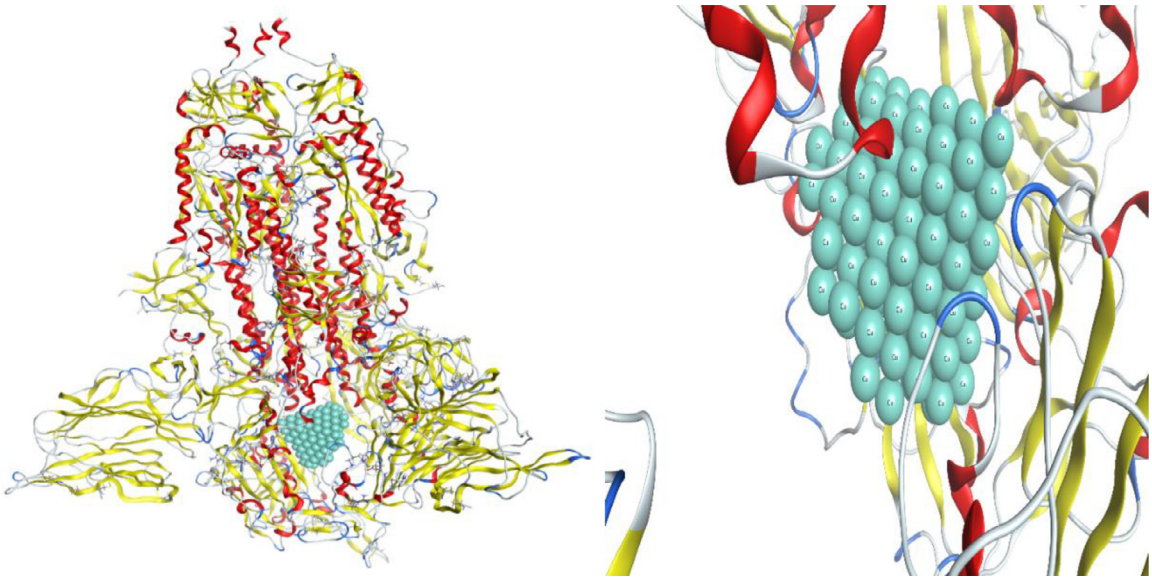

Figure 13. Schematic of the molecular docking between the Conical Copper NPs ligand and the 6ZGG receptor along with the pharmacophore drawn by MOE 2011.

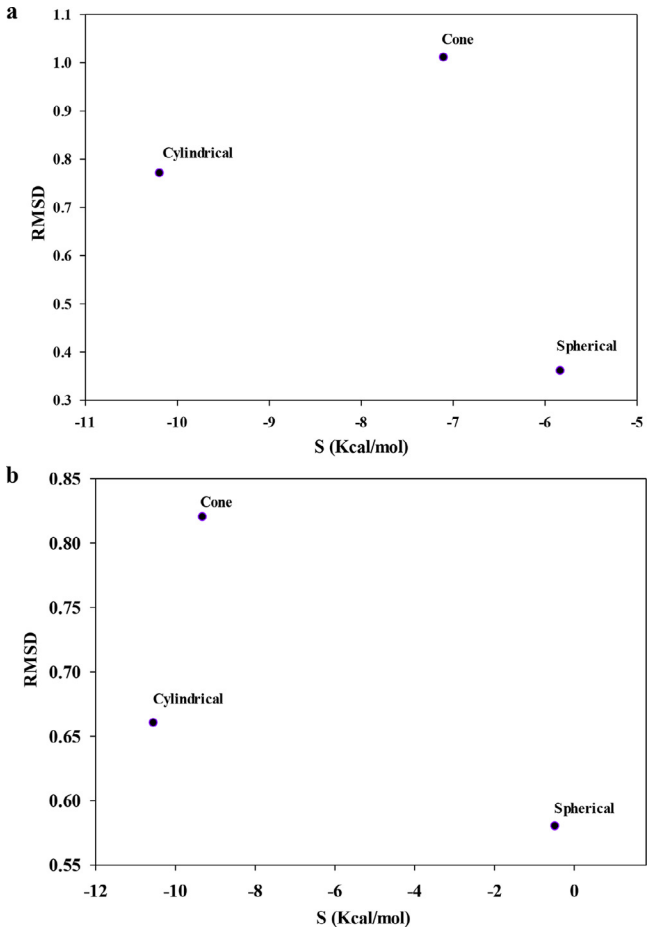

Figure 14. RMSD calculations of NPs Cu (Spherical, Cylindrical and Cone) with (a); 6M03 and (b); 6ZGG.

and cylindrical copper nanoparticles are more stable than spherical copper nanoparticles. Moreover, the RMSD and RMSF diagrams obtained from 6M03 and chain A (6ZGG) molecular dynamics. They are main parameters of molecular dynamics in order to balance

Table 7
Resulted parameters of redocking from interaction between copper NPs ligands and SARS-COV-2 main protease of MVD

Compound	Mol dock Score	ET
cone copper NPs	-169.465	-125.136
cylindrical copper NPs	-106.932	-101.24
spherical copper NPs	-65.674	-32.664

the system. The RMSD and RMSF diagrams from the molecular dynamics of 6M03 showed that the system had an RMSD = 0.25 nm at 75 nanoseconds. High levels of RMSF also imply the flexibility of 6M03 protein. RMSF fluctuations are between 0.1-0.3, indicating system stability over time. The RMSD and RMSF diagrams from Chain A (6ZGG) molecular dynamics also showed that the system has RMSD = 2 nm at 95 nanoseconds. High RMSF also imply chain A flexibility (6ZGG). RMSF fluctuations are between 0.25-0.8, indicating system stability over time.

The RMSD and RMSF diagrams of 6M03 and chain A of 6ZGG proteins were shown in Figure 17 and Figure 18, respectively.

3.5. MVD Molecular redocking studies related to M^{pro} and Chain A spike glycoprotein

For this purpose, molecular redocking of the ligands was performed in the active site where redocking had been carried out using the output file obtained from the molecular dynamics of 6M03 and chain A (6ZGG) and the best conformation of ligand or the Pose, the energy of which was minimum with the receptors, was selected and analyzed.

The binding energy of molecular redocking between the copper NPs ligands and the 6M03 and 6ZGG (chain A) targets were shown in Tables 7 and 8, respectively. In Figures 19a and d interactions of spherical copper NPs molecule with Ile 249, Pro 108 and Gln 110of 6M03 with a redocking score -65.674 Kcal/mol was shown. Conical copper NPs interacted with 6M03 (Figures 19b and e) with a redocking score -169.465 Kcal/mol and amino acid residues like Lys 5, Ala 7, Ser 123, Gly 124, Val 125, Tyr 126, Ser 139 and Glu 290. The resulted data from redocking analysis in Figures 19c and f show that cylindrical copper NPs interacted with amino acids of the 6M03 using Ser 10, Met 6 and Val 125 with redocking -106.932

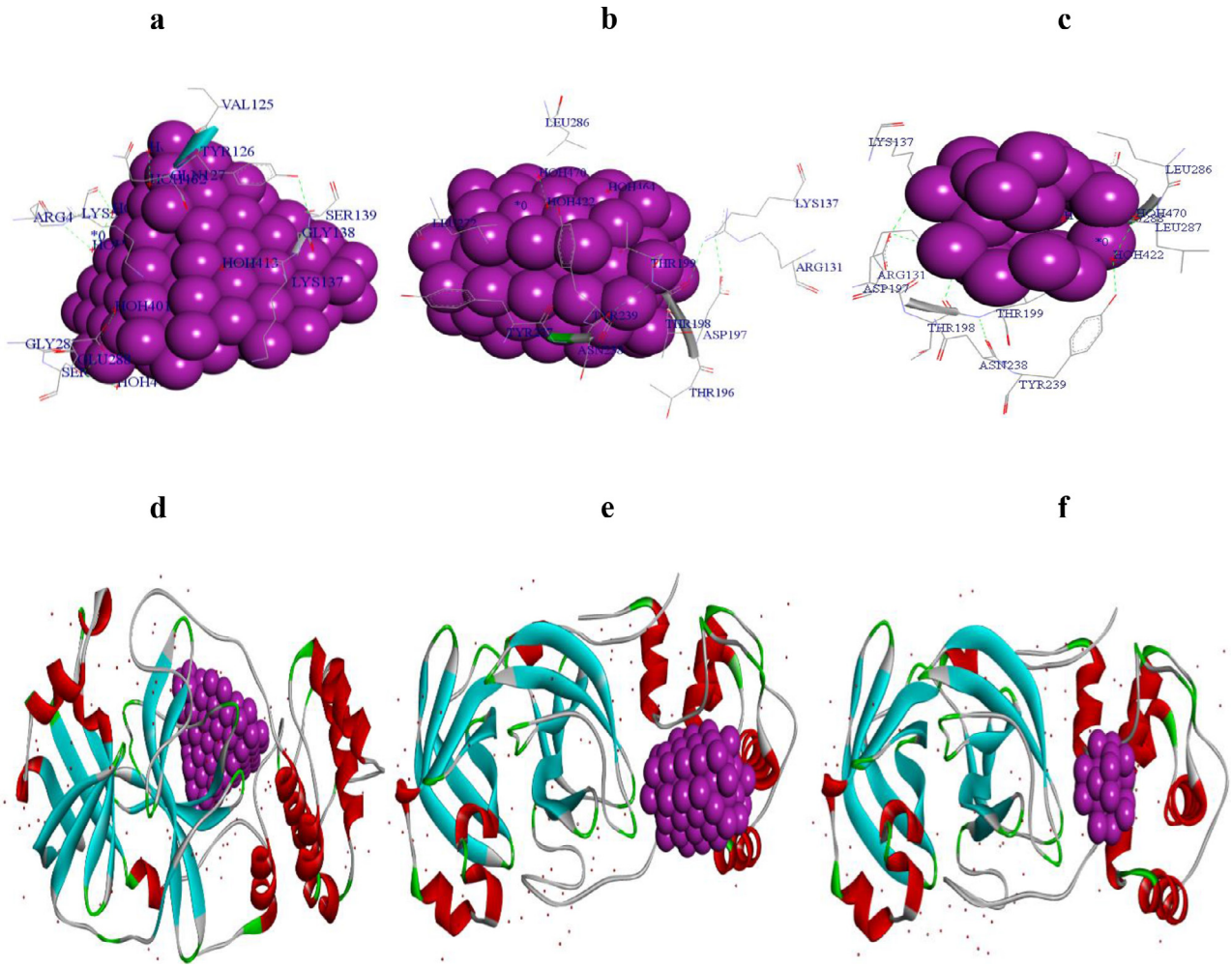

Figure 15. Schematic of the molecular docking between the Copper NPs ligands and the 6M03 receptor along with the pharmacophore and ligand map drawn by Discovery Studio.

Table 8
Resulted parameters of redocking from interaction between copper NPs ligands and SARS-COV-2 spike glycoprotein Chain A of MVD.

Compound	Mol dock Score	ET
Cone Copper NPs	-181.056	-122.305
Cylindrical Copper NPs	-118.036	-80.064
Spherical Copper NPs	-69.184	-8.766

Table 9
The best result of the redocking from interaction between copper NPs ligands and SARS-COV-2 main protease based on S, RMSD and E-refine of MOE.

E-refine (Kcal/mol)	RMSD	S (Kcal/mol)	Compound
-3.31	0.87	-3.31	cone copper NPs
-8.27	0.88	-8.27	cylindrical copper NPs
-12.15	1.19	-12.15	spherical copper NPs

Table 10
The best result of the redocking from interaction between copper NPs and SARS-COV-2 spike glycoprotein Chain A based on S, RMSD and E-refine of MOE.

E-refine (Kcal/mol)	RMSD	S (Kcal/mol)	Compound
1714.47	0.56	1714.47	cone copper NPs
-5584.98	2.00	-5584.98	cylindrical copper NPs
-11147.23	1.47	-11147.23	spherical copper NPs

score Kcal/mol. Furthermore, spherical copper NPs forms were stabilized by 6ZGG (chain A) (Figure 20a and d) with a redocking score of -69.184 Kcal/mol and using amino acid residues: Ile 418, Lys 417, Leu 455 and Tyr 489.

Likewise, redocking results were shown in Figure 20b and e conical copper NPs interacted with amino acids of the 6ZGG (chain A) using Tyr 28, Phe 59, Phe 138, Leu 293, Ser 383, Thr 385 and Ala 570 with a redocking score -181.056 Kcal/mol. cylindrical Copper NPs using amino acid residues: Asn 61, Tyr 269, Gln 271, Gly 381, Ser 383, Lys 386, Ala 570 and Asp 571 of 6ZGG (chain A) (Figure 20c and f) was stabilized with a redocking score of -118.036 Kcal/mol.

Consequently, the redocking results indicated that conical copper NPs and cylindrical copper NPs were more efficient than spherical copper NPs to 6M03 and 6ZGG (chain A). Relevant tables in which energy and redocking score were written in the article, implied that conical copper NPs had the best results of redocking.

3.6. MOE Molecular redocking studies related to M^{pro} and chain A spike glycoprotein

The redocking results are listed in Tables 9 and 10. Figures of 21 and 22 display the ligand map and pharmacophore of molecu-

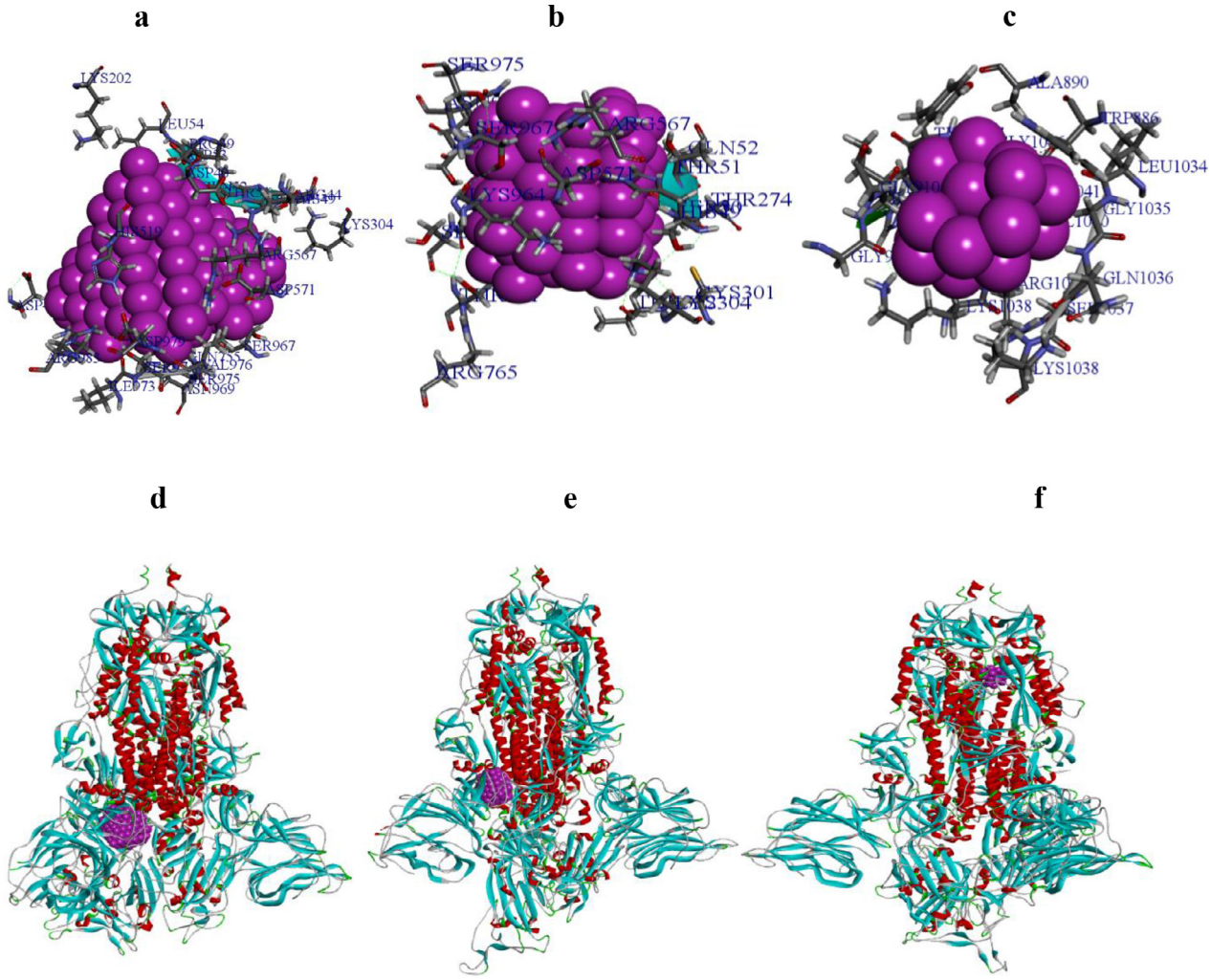

Figure 16. Schematic of the molecular docking between the Copper NPs ligands and the 6ZGG receptor along with the pharmacophore and ligand map drawn by Discovery Studio.

lar redocking between the copper NPs ligands and the 6M03 and Chain A (6ZGG) targets in MOE. Figures 21a and b showed interactions of spherical copper NPs molecule with Leu A286, Glu A288, Thr A199, Lys A137, Tyr A 239, Asp A197, Asn A 238, Tyr A237 amino acid residues from 6M03 receptor. Figures 21c and d show interactions of cylindrical copper NPs molecule with Glu A166, Asn A119, Thr A24, Thr A26, Thr A25, Gly A143, Leu A27, Cys A 44, Thr A45, Asn A142, His A41, Ser A46, Gln A 189 and Pro A168 amino acid residues from 6M03 receptor. Figures 21e and f show interacted conical copper NPs molecule with Gly A283, Val A125, Lys A5, Glu A14 amino acid residues from receptor 6M03.

Figures 22a and b show interactions of spherical copper NPs molecule with Leu A894, Met A900, Ile A896, Ala A903, Gln A901, Gln A913, Tyr A917, Asn A907 and Tyr A904 amino acid residues from chain A of 6ZGG receptor. Figures 22c and d show interactions of cylindrical copper NPs molecule with Leu A293, Pro A57, Pro A272, Arg A273, Ala A292, Gln A271, Leu 293, Ser A316, Asn A317, Ile A569, Phe A318, Arg A 319 and Ala A570 amino acid residues from chain A of 6ZGG receptor. Figures 22e and f is show interacted conical copper NPs molecule with Lys A386, ThrA385, Asn A61, Tyr A269, Gln A271, Pro A57, Arg A273 and Phe A318 amino acid residues from receptor Chain A 6ZGG.

The calculated minimum relative Free Total Energy values score suggest that they reasonably involved with macromolecules. Comparing the Free Total Energy of compounds with main protease and Chain A (6ZGG) that conical copper NPs was more effective than other compounds to main protease and spike glycoprotein.

Table 11
Resulted parameters of the redocking from interaction between copper NPs ligands and SARS-COV-2 main protease of Autodock Vina.

Compound	affinity(Kcal/mol)
Cone Copper NPs	-13.5
Cylindrical Copper NPs	-12.0
Spherical Copper NPs	-7.9

3.7. Autodock Vina Molecular redocking studies related to M^{pro} and chain A of spike glycoprotein

Conformation of redocked copper NPs ligand with main protease and chain A (6ZGG) were analyzed in terms of affinity values and were dominated by the negative energy values, implying that the binding effects of the compounds were spontaneous. The results were reported in Table 11 and the values of Energy of affinity

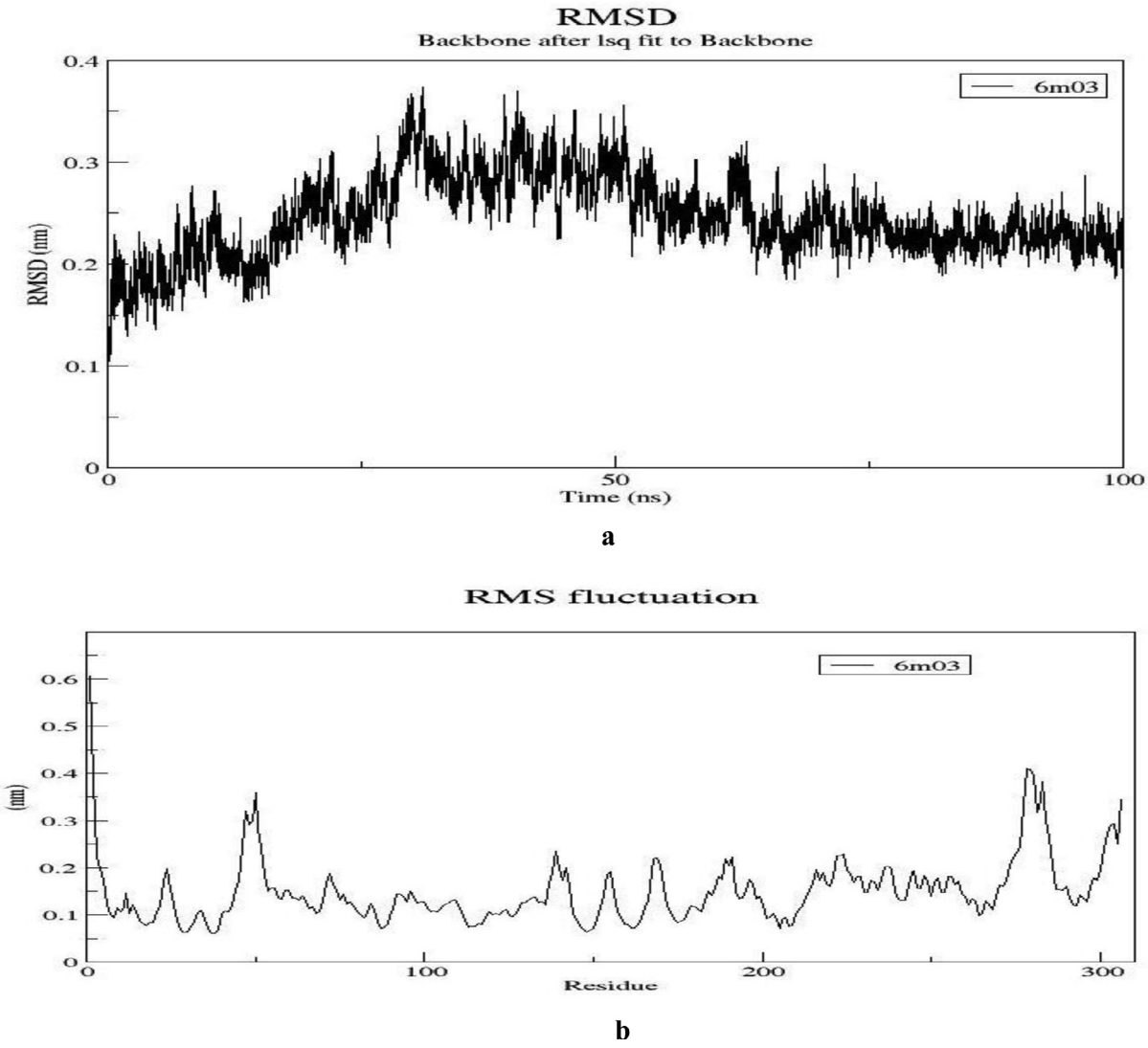

Figure 17. a) The root mean square deviation (RMSD) value and b) RMSF (root mean square fluctuation) of M^{pro} SARS-COV-2.

Table 12
Resulted parameters of the redocking from interaction between Copper NPs ligands and SARS-COV-2 spike glycoprotein Chain A of Autodock Vina.

Compound	affinity(Kcal/mol)
Cone Copper NPs	-19.2
Cylindrical Copper NPs	-18.5
Spherical Copper NPs	-8.8

were -13.5, -12.0 and -7.9 for conical, cylindrical and spherical copper NPs docked to main protease respectively. The data in Table 12 show that affinity of conical cylindrical and spherical copper NPs interacted with chain A (6ZGG) was -19.2, -18.5 and -8.8 respectively. The calculated minimum relative affinity values score suggest that they reasonably interacted with macromolecules. Comparing the affinity of compounds with main protease and Chain A (6ZGG) that conical copper NPs was more effective than other compounds to main protease and chain A (6ZGG).

Figures 23 a-f show the highest level of interactions of copper NPs ligand at the active site of main protease. The resulted data from redocking analysis showed that conical Copper NPs interacted with amino acids of the main protease (PDB ID, 6M03) using Ser A139, Glu A 288, Glu A290, Gln A127, Tyr A126, Val A125, Gly A124, Ser A123, Tyr A118, Pro A122, Glu A14, Ser A10, Phe A 8, Met A6, Ala A7 and Lys A5 (Figures 23 a and d). Cylindrical copper NPs interacted with amino acid residues Asn A133, Asn A238, Asp A197, Arg A131, Thr A135, Val A171, Gly A170, Ile A136, His A172, Lys A137, Gly A138, Phe A140 and Ser A139 in active site of main protease (Figures 23 b and e). Meanwhile, interactions between the spherical copper NPs and main protease were dominated by Lys A137, Asp A289, Glu A 288, Leu A 286, Arg A131, Asp A197, Thr A199, Asn A238, Tyr A239 in Figure 23 c and f.

Interactions of copper NPs with residues of chain A (6ZGG) were shown in Figures 24 a-c. Figures 24 d-f indicates copper NPs embedded in the active site of chain A (6ZGG). Also, conical Copper NPs interacted with Gln A 992, Ile A973, Ala A972, Gly A971, Ser A974, Asn A969, Ser A975, Gln A52, Thr A51, Asp A53, Leu A54, Arg A44, Pro A39, Asp A40, Val A42, Ile A197, Asp A198, Lys A195

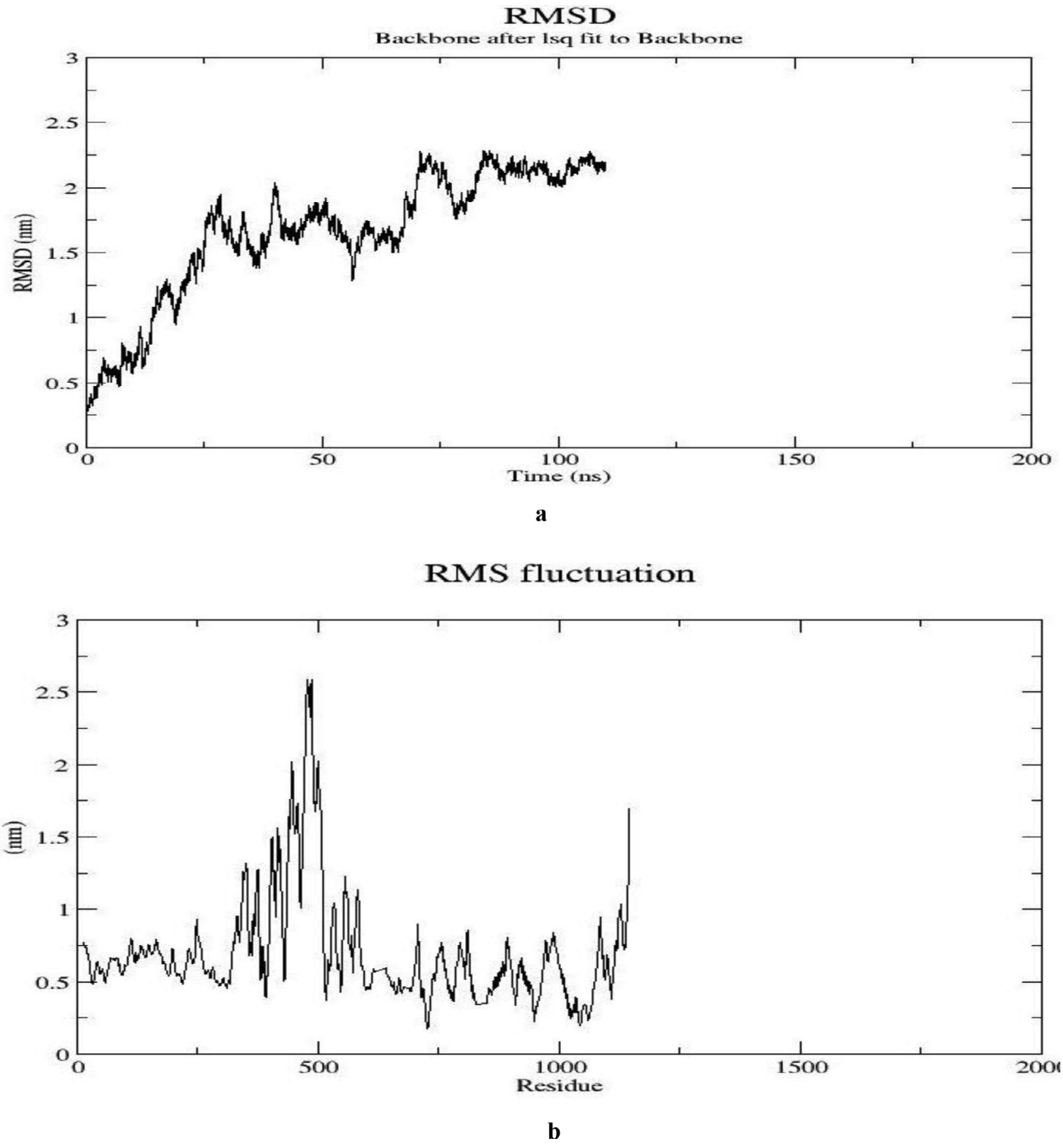

Figure 18. a) The root means square deviation (RMSD) value and b) RMSF (root mean square fluctuation) of spike glycoprotein chain A SARS-COV-2 (6ZGG).

and His A49 to chain A (6ZGG) respectively. Cylindrical copper NPs was redocked into Spike glycoprotein using Arg A983, Asp A979, Lys A41, Val A42, Asp A40, Pro A39, Asp A53, Gln A52, Arg A44, ser A974, Ile A973, Ala A972, Ser A975, Gly A971, Asn A969, His A49, Ser A50 and Thr A51. Spherical Copper NPs/spike glycoprotein complex interacted with Leu A977, Ser A746, Val A976, Ser A975, Arg A44, Ser A45, Ser A967, Ser A46, Val A47, Leu A966, Arg A1000, Cys A743, Gly A744, Ile A742, Thr A739, Met A740, Tyr A741.

3.8. Recent studies on the antimicrobial and antiviral properties of copper

Recent investigations have found novel and effective ways of decreasing the risk of transmission of several respiratory viruses such as the Coronaviridae and influenza family, for instance using of copper [13,22–28]. Copper has been used in clinical settings to reduce the risk of bacterial and viral contamination, complementing traditional protocols. Furthermore, adding copper nanoparticles

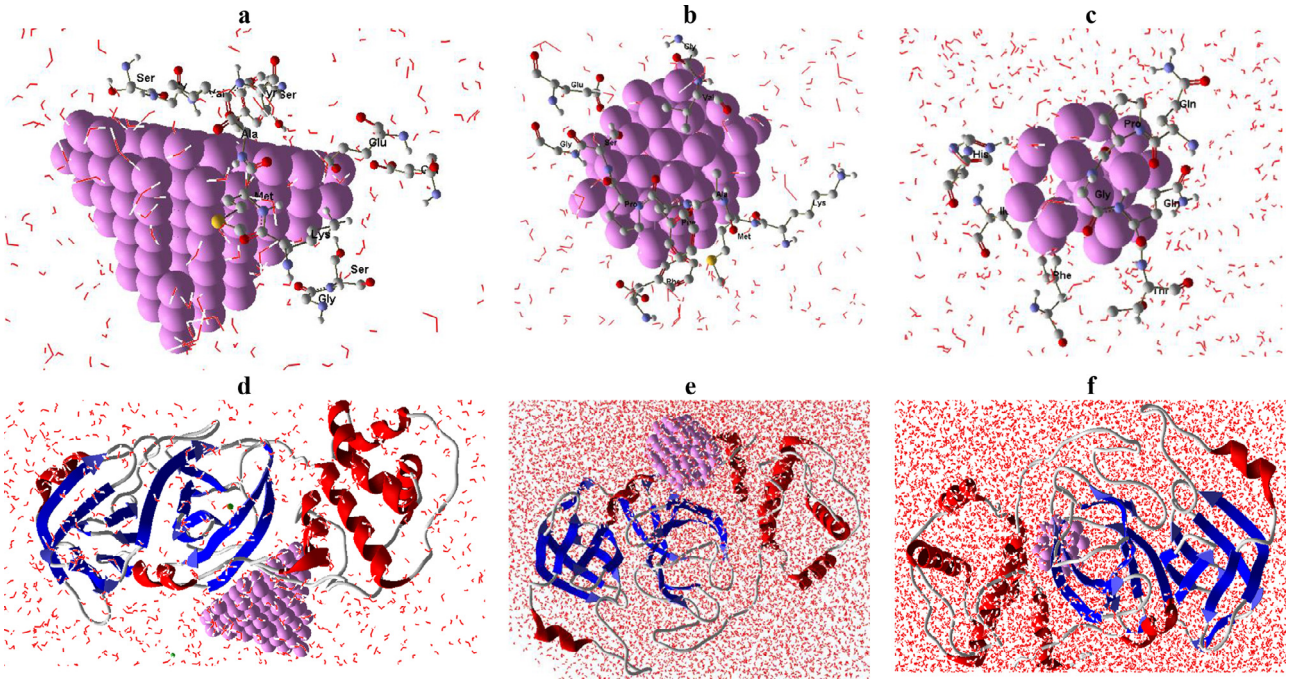

Figure 19. Schematic of the molecular redocking Molecular Dynamics between the cylindrical copper NPs ligand and the 6M03 receptor along with the pharmacophore drawn by MVD 6.0.

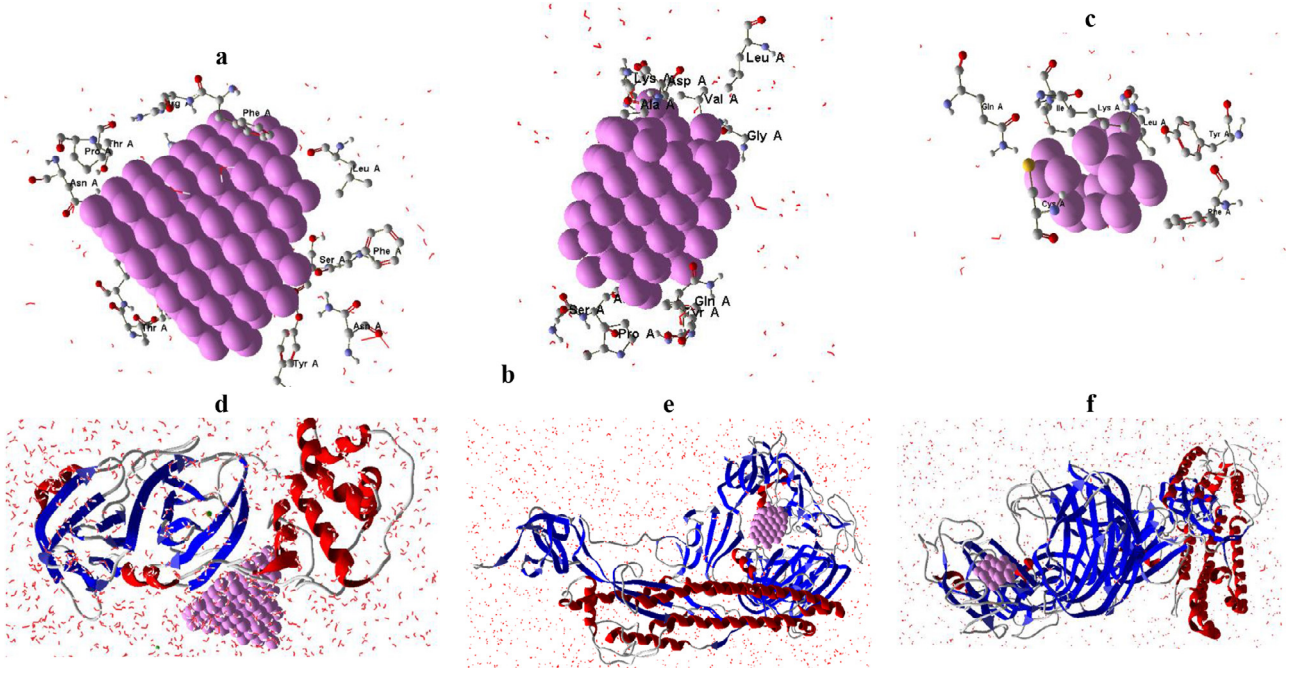

Figure 20. Schematic of the molecular redocking Molecular Dynamics between the cylindrical copper NPs ligand and the chain A of 6ZGG receptor along with the pharmacophore drawn by MVD 6.0.

to polymer/plastic matrices can also produce highly effective antimicrobial materials. A various type of respiratory pathogens such as influenza, SARSCoV, MERS-CoV, and HCoV have been exposed to a variety of copper forms in several cultivating media. The results implicate that, copper is capable of inhibition, inactivation, reduction, and irreversible destruction of coronavirus, influenza virus, and other pathogenic microorganisms in a matter of minutes. A recent study has evaluated and compared SARS-CoV-1 and SARS-CoV-2 stability and the rate of aerosols decay, in the presence of copper (metallic plate at 99% of copper), cardboard, stainless steel, and plastic, these data may probably suggest that copper has more significant effect on SARS-CoV-2.

The previous or provided data appear to support the use of copper in different ways in order to inactivate viruses (and a wide

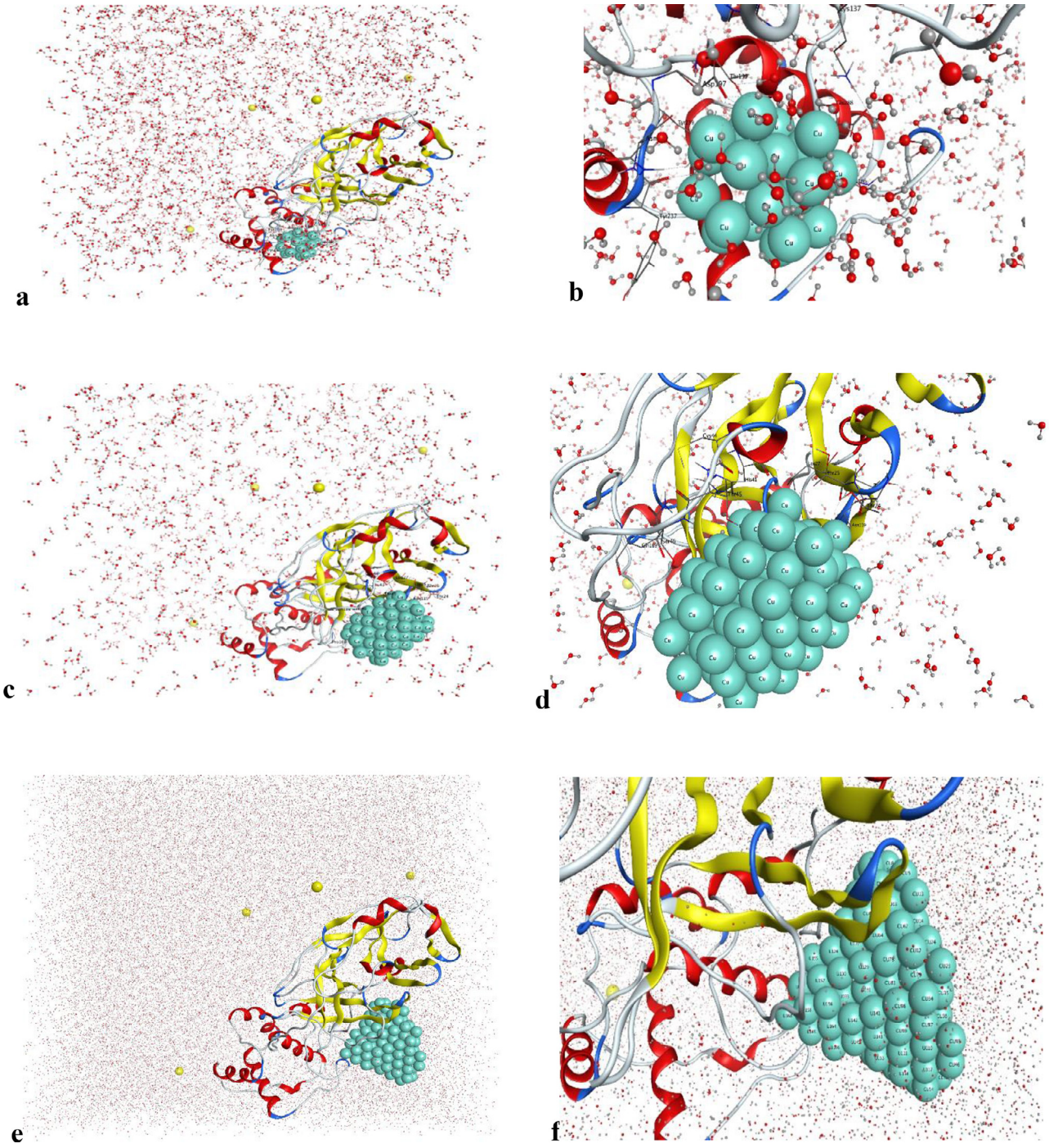

Figure 21. Schematic of the molecular redocking Molecular Dynamics between the Cylindrical copper NPs ligand and the 6M03 receptor along with the pharmacophore drawn by MOE 2011

range of microorganisms)actively, and it seems to be an effective and affordable strategy to help reducing transmission of several infectious diseases such as the coronavirus, despite the genetic similarities, more research would be beneficial to support its usage with the new SARS-Cov-2 [29,30].

According to recent research, copper was used to inhibit the protease of human immunodeficiency [31]. The role of copper in inactivation of influenza A was confirmed. Cu can inactivate several infectious viruses such as bronchitis virus, poliovirus, human immunodeficiency virus type 1(HIV-1), other enveloped or nonenveloped, single- or double-stranded DNA and RNA viruses. Moreover, Cu has the potent capacity of inactivating SARS-CoV-2. Since the current outbreak of the COVID-19 pandemic, furthermore copper is also recognized as a potent antibacterial particle agent. Its application in particle form (especially Nano particles) shows very interesting properties.so it can be concluded that using(application) of copper in particle forms can be very helpful to control covid 19 pandemic [32] so it can be concluded that using(application) of copper in particle forms can be very helpful to control covid 19 pandemic [1-3]. Therefore, it can be

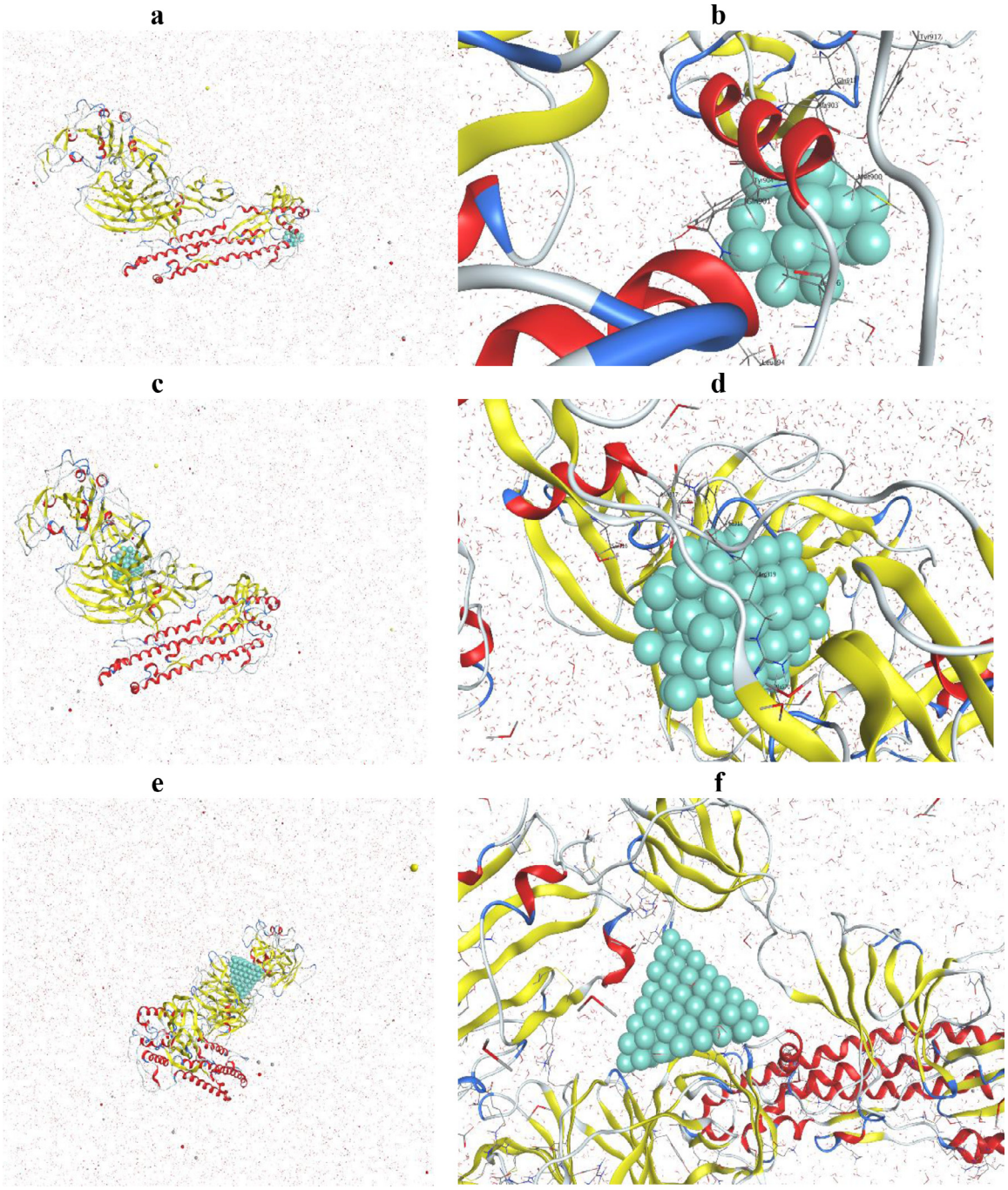

Figure 22. Schematic of the molecular redocking Molecular Dynamics between the cylindrical copper NPs ligand and the chain A of 6ZGG receptor along with the pharmacophore drawn by MOE 2011

very helpful to control covid 19 pandemic which is still a global challenge.

Shape/size dependence on LSPR of noble metal nano structures have been extensively investigated, and easily controlled, e. g.; for golden nano rods, the LSPRs expand within 500–1100 nm via controlling the aspect ratio [33–35] the LSPR energy of copper chalcogenide NCs is dependent on shape parameters (e. g.; aspect ratio), besides charge carrier density. Tao et al. reported for the first time the observation of size/shape dependent LSPRs for Cu_2-xS Nano disks that possess in-plane and out-of-plane dipoles associated with the ultra-thin disk geometry, in which two extinction bands near 1800and 3100 nm were observed. This is different from Cu_2-xSnanospheres, which show only one LSPR peak at 1550 nm.[36]. Focus on factors that impact their localized surface Plasmon resonances (LSPRs) and on methods used for tuning the LSPRs [37].

The antimicrobial activity of nanoparticles increases according to their size and the most important of them are different forms of metal NPs, as shown in Tables 1-12.

Currently, in the mortal conditions caused by the corona virus, the use of drug simulation and design can minimize the time required to identify and design drug compounds andtheir types, and optimize their structure in addition it helps reduce the cost of laboratory processes and materials This technology also speeds up drug design and discovery, as well as improving drug performance.

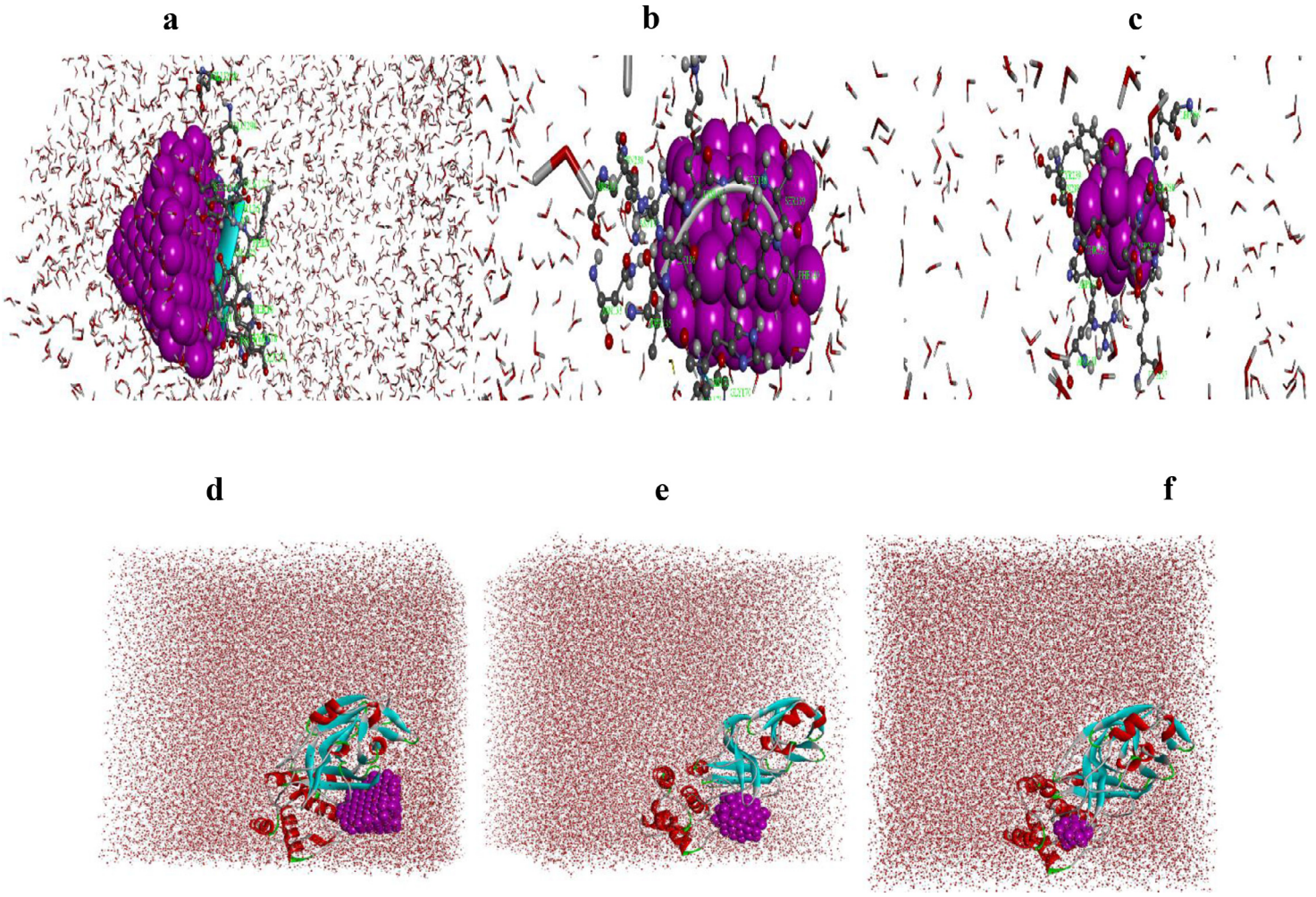

Figure 23. Schematic of the molecular redocking Molecular Dynamics between the copper NPs ligands and the 6M03 receptor along with the pharmacophore and ligand map drawn by Discovery Studio.

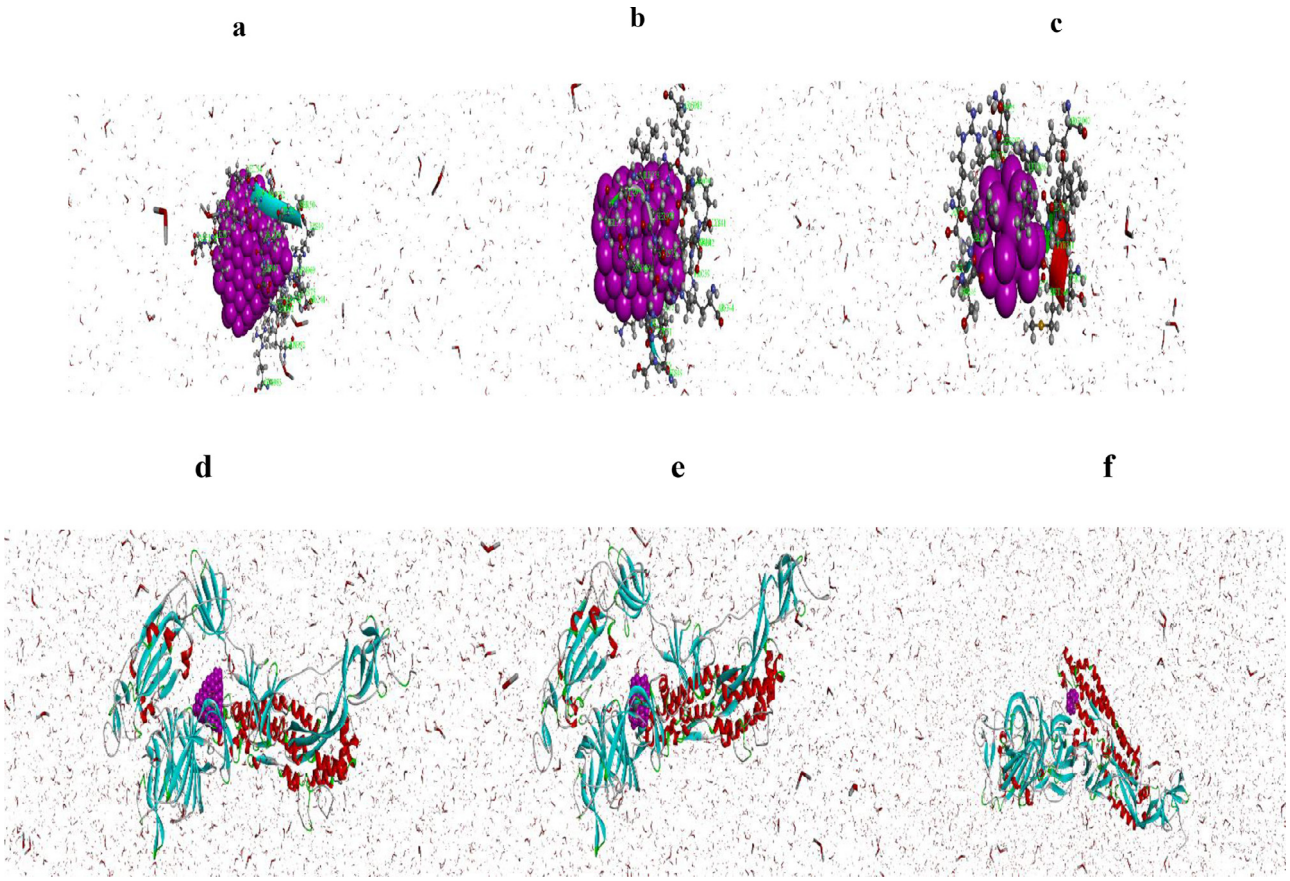

Figure 24. Schematic of the molecular redocking Molecular Dynamics between the copper NPs ligands and the chain A of 6ZGG along with the pharmacophore and ligand map drawn by Discovery Studio.

4. Conclusion

In this research, the effect of copper NPs with different shapes (spherical, cylindrical and conical) for docking with coronavirus protease and spike glycoprotein (6M03 and 6ZGG) was analyzed. The evaluation of antiviral effect of this nano-structure revealed that nanoparticles of Cu could block a key enzyme that helps viruses replicate. In fact, nanoparticles of Cu were such as protease and spike glycoprotein inhibitors. The distribution of electron density of copper NPs showed that copper NPs react electrostatically with corona virus protease and spike glycoprotein. The docking results showed us that cylindrical and conical copper NPs were more efficient than spherical copper NPs. Relevant tables, energy and docking scoring, which were mentioned in the article, also showed that cylindrical and conical copper NPs had the best results of docking. Therefore, the shape of nanoparticles was very important in influencing virus protease spike glycoprotein.to conclude copper NPs can be used to disinfect surfaces.

The results of molecular redocking showed that the complexes formed between the studied ligands and receptors were more stable than in the case where that docking without MD was performed. As result, the energy of conical copper NPs is more negative than cylindrical copper NPs indicating the higher level of stability of conical form. It is also proved in molecular dynamics and then molecular docking that cylindrical form is better than spherical nanoparticles.

Furthermore, the RMSD and RMSF values also indicate that there is a small computational error, implying that the considered system has reached equilibrium.

This study aimed to use copper NPs as a disinfectant for SARS virus and extensive studies in the field of copper NPs suggest that this agent can be used as a disinfectant in hospitals, government departments and public places.

Credit Author Statement

The descriptions are accurate and agreed by All authors. All authors contributed to the study conception and design. Material preparation, data collection and analysis were performed by Mohammadreza Aallaei, Elaheh Molaakbari, Navvabeh Salarizadeh, and Rahime Eshaghi Maleksah. The first draft of the manuscript was written by Mohammadreza Aallaei, Elaheh Molaakbari and Navvabeh Salarizadeh and other authors commented on previous versions of the manuscript. All authors read and approved the final manuscript.

Declaration of Competing Interest

The authors declare that they have no known competing financial interests or personal relationships that could have appeared to influence the work reported in this paper

Supplementary materials

Supplementary material associated with this article can be found, in the online version, at doi:10.1016/j.molstruc.2021.132301.

References

[1] R. Swanstrom, J. Anderson, C. Schiffer, S.K. Lee, Viral protease inhibitors, Handbook of Experimental Pharmacology 189 (2009), doi:10.1007/978-3-540-79086-0_4.

[2] F. Wu, S. Zhao, B. Yu, Y.M. Chen, W. Wang, Z.G. Song, Y. Hu, Z.W. Tao, J.H. Tian, Y.Y. Pei, M.L. Yuan, Y.L. Zhang, F.H. Dai, Y. Liu, Q.M. Wang, J.J. Zheng, L. Xu, E.C. Holmes, Y.Z. Zhang, A new coronavirus associated with human respiratory disease in China, Nature (2020) 579, doi:10.1038/s41586-020-2008-3.

[3] S. Jo, S. Kim, D.H. Shin, M.S. Kim, Inhibition of SARS-CoV 3CL protease by flavonoids, Journal of Enzyme Inhibition and Medicinal Chemistry 35 (2020), doi:10.1080/14756366.2019.1690480.

[4] L. Du, Y. He, Y. Zhou, S. Liu, B.J. Zheng, S. Jiang, The spike protein of SARS-CoV - A target for vaccine and therapeutic development, Nature Reviews Microbiology 7 (2009), doi:10.1038/nrmicro2090.

[5] Z. Song, Y. Xu, L. Bao, L. Zhang, P. Yu, Y. Qu, H. Zhu, W. Zhao, Y. Han, C. Qin, From SARS to MERS, thrusting coronaviruses into the spotlight, Viruses 11 (2019), doi:10.3390/v11010059.

[6] M. Wang, R. Cao, L. Zhang, X. Yang, J. Liu, M. Xu, Z. Shi, Z. Hu, W. Zhong, G. Xiao, Remdesivir and chloroquine effectively inhibit the recently emerged novel coronavirus (2019-nCoV) in vitro, Cell Research 30 (2020), doi:10.1038/s41422-020-0282-0.

[7] C.C. Lai, T.P. Shih, W.C. Ko, H.J. Tang, P.R. Hsueh, Severe acute respiratory syndrome coronavirus 2 (SARS-CoV-2) and coronavirus disease-2019 (COVID-19): The epidemic and the challenges, International Journal of Antimicrobial Agents 55 (2020), doi:10.1016/j.ijantimicag.2020.105924.

[8] Z. Wang, X. Chen, Y. Lu, F. Chen, W. Zhang, Clinical characteristics and therapeutic procedure for four cases with 2019 novel coronavirus pneumonia receiving combined Chinese and Western medicine treatment, BioScience Trends 14 (2020), doi:10.5582/BST.2020.01030.

[9] G. Li, E. de Clercq, Therapeutic options for the 2019 novel coronavirus (2019-nCoV), Nature Reviews, Drug Discovery 19 (2020), doi:10.1038/d41573-020-00016-0.

[10] X. Yao, F. Ye, M. Zhang, C. Cui, B. Huang, P. Niu, X. Liu, L. Zhao, E. Dong, C. Song, S. Zhan, R. Lu, H. Li, W. Tan, D. Liu, In vitro antiviral activity and projection of optimized dosing design of hydroxychloroquine for the treatment of severe acute respiratory syndrome coronavirus 2 (SARS-CoV-2), Clinical Infectious Diseases 71 (2020), doi:10.1093/cid/ciaa237.

[11] L. Zhang, Y. Liu, Potential interventions for novel coronavirus in China: A systematic review, Journal of Medical Virology 92 (2020), doi:10.1002/jmv.25707.

[12] L. Zhang, D. Lin, Y. Kusov, Y. Nian, Q. Ma, J. Wang, A. von Brunn, P. Leyssen, K. Lanko, J. Neyts, A. de Wilde, E.J. Snijder, H. Liu, R. Hilgenfeld, α-Ketoamides as Broad-Spectrum Inhibitors of Coronavirus and Enterovirus Replication: Structure-Based Design, Synthesis, and Activity Assessment„ Journal of Medicinal Chemistry 63 (2020), doi:10.1021/acs.jmedchem.9b01828.

[13] Y. Fujimori, T. Sato, T. Hayata, T. Nagao, M. Nakayam, T. Nakayam, R. Sugamat, K. Suzuki, Novel antiviral characteristics of nanosized copper(i) iodide particles showing inactivation activity against 2009 pandemic H1N1 influenza virus, Applied and Environmental Microbiology 78 (2012), doi:10.1128/AEM.06284-11.

[14] J.O. Noyce, H. Michels, C.W. Keevil, Inactivation of influenza A virus on copper versus stainless steel surfaces, Applied and Environmental Microbiology 73 (2007), doi:10.1128/AEM.01139-06.

[15] A. Amtmann, I. Ahmed, P. Zahner-Rimmel, A. Mletzko, L.K. Jordan, M. Oberle, H. Wedekind, J. Christian, S.M. Bergmann, A.M. Becker, Virucidal effects of various agents—including protease—against koi herpesvirus and viral haemorrhagic septicaemia virus, Journal of Fish Diseases 43 (2020), doi:10.1111/jfd.13106.

[16] T. Kruk, K. Szczepanowicz, J. Stefańska, R.P. Socha, P. Warszyński, Synthesis and antimicrobial activity of monodisperse copper nanoparticles, Colloids and Surfaces B: Biointerfaces 128 (2015), doi:10.1016/j.colsurfb.2015.02.009.

[17] T. Ishida, Antiviral Activities of Cu $^{2+}$ Ions in Viral Prevention, Replication, RNA Degradation, and for Antiviral Efficacies of Lytic Virus, ROS-Mediated Virus, Copper Chelation, World Scientific News 99 (2018).

[18] R. Chawla, S. Sharma, Molecular dynamics simulation of carbon nanotube pullout from polyethylene matrix, Composites Science and Technology 144 (2017), doi:10.1016/j.compscitech.2017.03.029.

[19] K. Rawal, T. Khurana, H. Sharma, S. Verma, S. Gupta, C. Kubba, U. Strych, P.J. Hotez, M.E. Bottazzi, An extensive survey of molecular docking tools and their applications using text mining and deep curation strategies (2019), doi:10.7287/peerj.preprints.27538.

[20] T.F. Vieira, S.F. Sousa, Comparing AutoDock and Vina in ligand/decoy discrimination for virtual screening, Applied Sciences (Switzerland) 9 (2019), doi:10.3390/app9214538.

[21] N.S. Pagadala, K. Syed, J. Tuszynski, Software for molecular docking: a review, Biophysical Reviews 9 (2017), doi:10.1007/s12551-016-0247-1.

[22] K. Imai, H. Ogawa, V.N. Bui, H. Inoue, J. Fukuda, M. Ohba, Y. Yamamoto, K. Nakamura, Inactivation of high and low pathogenic avian influenza virus H5 subtypes by copper ions incorporated in zeolite-textile materials, Antiviral Research 93 (2012), doi:10.1016/j.antiviral.2011.11.017.

[23] A. Ito, A. Tsuneki, Y. Yoshida, K. Ryoke, T. Kaidoh, S. Kageyama, In vitro inhibition of cytopathic effect of influenza virus and human immunodeficiency virus by bamboo leaf extract solution and sodium copper chlorophyllin, Yonago Acta Medica 59 (2016).

[24] A. Majbauddin, I. Kodani, K. Ryoke, The effect of bamboo leaf extract solution and sodium copper chlorophyllin solution on growth and volatile sulfur compounds production of oral malodor associated some anaerobic periodontal bacteria, Yonago Acta Medica 58 (2015).

[25] M. Minoshima, Y. Lu, T. Kimura, R. Nakano, H. Ishiguro, Y. Kubota, K. Hashimoto, K. Sunada, Comparison of the antiviral effect of solid-state copper and silver compounds, Journal of Hazardous Materials 312 (2016), doi:10.1016/j.jhazmat.2016.03.023.

[26] S.L. Warnes, Z.R. Little, C.W. Keevil, Human coronavirus 229E remains infectious on common touch surface materials, MBio 6 (2015), doi:10.1128/mBio.01697-15.

[27] S. Zerbib, L. Vallet, A. Muggeo, C. de Champs, A. Lefebvre, D. Jolly, L. Kanagaratnam, Copper for the Prevention of Outbreaks of Health Care–Associated Infections in a Long-term Care Facility for Older Adults, Journal of the American Medical Directors Association 21 (2020), doi:10.1016/j.jamda.2019.02.003.

[28] N. van Doremalen, T. Bushmaker, D.H. Morris, M.G. Holbrook, A. Gamble, B.N. Williamson, A. Tamin, J.L. Harcourt, N.J. Thornburg, S.I. Gerber, J.O. Lloyd-Smith, E. de Wit, V.J. Munster, Aerosol and Surface Stability of SARS-CoV-2 as Compared with SARS-CoV-1, New England Journal of Medicine 382 (2020), doi:10.1056/nejmc2004973.

[29] J.Valeria Prado, A.Roberto Vidal, T.Claudia Durán, Application of copper bactericidal properties in medical practice, Revista Medica de Chile 140 (2012), doi:10.4067/S0034-98872012001000014.

[30] S. Raha, R. Mallick, S. Basak, A.K. Duttaroy, Is copper beneficial for COVID-19 patients? Medical Hypotheses 142 (2020), doi:10.1016/j.mehy.2020.109814.

[31] A.R. Karlstrom, R.L. Levine, Copper inhibits the protease from human immunodeficiency virus 1 by both cysteine-dependent and cysteine-independent mechanisms, Proceedings of the National Academy of Sciences of the United States of America 88 (1991), doi:10.1073/pnas.88.13.5552.

[32] M. Vincent, R.E. Duval, P. Hartemann, M. Engels-Deutsch, Contact killing and antimicrobial properties of copper, Journal of Applied Microbiology 124 (2018), doi:10.1111/jam.13681.

[33] V. Juve, M.F. Cardinal, A. Lombardi, A. Crut, P. Maioli, L.M. Liz-Marzan, N. del Fatti, F. Vallee, Size dependent surface plasmon resonance broadening in non-spherical nanoparticles: Single gold nanorods, 2013 Conference on Lasers and Electro-Optics Europe and International Quantum Electronics Conference, CLEO/Europe-IQEC 2013, 2013, doi:10.1109/CLEOE-IQEC.2013.6801889.

[34] C.L. Nehl, J.H. Hafner, Shape-dependent plasmon resonances of gold nanoparticles, Journal of Materials Chemistry 18 (2008), doi:10.1039/b714950f.

[35] E. Ringe, J.M. McMahon, K. Sohn, C. Cobley, Y. Xia, J. Huang, G.C. Schatz, L.D. Marks, R.P. van Duyne, Unraveling the effects of size, composition, and substrate on the localized surface plasmon resonance frequencies of gold and silver nanocubes: A systematic single-particle approach, Journal of Physical Chemistry C 114 (2010), doi:10.1021/jp104366r.

[36] S.W. Hsu, K. On, A.R. Tao, Localized surface plasmon resonances of anisotropic semiconductor nanocrystals, Journal of the American Chemical Society 133 (2011), doi:10.1021/ja2089876.

[37] W. Xu, H. Liu, D. Zhou, X. Chen, N. Ding, H. Song, H. Ågren, Localized surface plasmon resonances in self-doped copper chalcogenide binary nanocrystals and their emerging applications, Nano Today 33 (2020), doi:10.1016/j.nantod.2020.100892.